

AFOSR-TR. 80-0251

① LEVEL II

PSI TR-204

ROUGH WALL REENTRY HEATING ANALYSIS

FINAL REPORT

EFFECT OF SURFACE ROUGHNESS CHARACTER
ON
TURBULENT BOUNDARY LAYER HEATING

February 1980

DTIC
ELECTE
MAR 31 1980
S B D

by

B

M.L. Finson, A.S. Clarke, and P.K.S. Wu

FINAL

Jointly Sponsored by

The Space and Missile Systems Organization
and
The Air Force Office of Scientific Research (AFSC)

Contract F49620-78-C-0028

ADA 082438

PHYSICAL SCIENCES INC.

30 COMMERCE WAY, WOBURN, MASS. 01801

DISTRIBUTION STATEMENT A

Approved for public release;
Distribution Unlimited

86 3 20 002

6

ROUGH WALL REENTRY HEATING ANALYSIS
FINAL REPORT
Effect of Surface Roughness Character
on Turbulent Boundary Layer Heating

11

February, 1980

12

56

9 Final Rpt. 1160-77-3007 7/13

10

by
M.L. Finson / A.S. Clarke / P.K.S. Wu

Jointly Sponsored by

The Space and Missile Systems Organization
and
The Air Force Office of Scientific Research (AFOSR)

15

Contract F49620-78-C-0028

16 SEP 11

17 A 11

18 AFOSR

19

77-80-020-1

DISTRIBUTION STATEMENT A
Approved for public release;
Distribution Unlimited

1371-105

47

ABSTRACT

A Reynolds stress model is used to evaluate the effect of surface roughness on turbulent boundary layers. Roughness is represented by distributed source or sink terms in the various governing equations, the most important term being a sink term in the mean momentum equation describing form drag on the roughness elements. The blockage effect of closely spaced elements is treated by accounting for the volume fraction occupied by the solid material. Calculations based on the theory have been compared with the available data on the influence of roughness character, where the roughness shape and spacing were varied. Reasonable agreement was obtained against most of Schlichting's low speed data with spherical, spherical segment, and conical roughness elements at various spacings. The cone measurements imply a somewhat higher effective drag coefficient than observed on the other shapes. The second set of experiments that were analyzed in detail were performed by Acurex under supersonic conditions, with a number of roughnesses created by grit or chemical etching processes. The heat transfer data and the present theory indicate spacing to be more important than height under the conditions tested. Analysis of the computer results reveals that the mean velocity is nearly constant over much of the height range $y < k$. This in turn indicates that the projected roughness element area per unit superficial area is a key scaling parameter. The "plateau" velocity is found to depend primarily on relative roughness spacing, and methods are suggested for developing better approximate techniques for predicting roughness character effects. Finally, preliminary data on hypersonic rough wall turbulent boundary layers have been examined with the present theory.

AIR FORCE
G...
... (AFOSR)
...
...
A. D. ...
Technical Information Officer

Conditions of Reproduction

Reproduction, translation, publication, use and disposal in whole or in part by or for the United States Government is permitted.

ACCESSION for	
NTIS	White Section <input checked="" type="checkbox"/>
DDC	Buff Section <input type="checkbox"/>
UNANNOUNCED	<input type="checkbox"/>
JUSTIFICATION _____	
BY _____	
DISTRIBUTION/AVAILABILITY CODES	
Dist: AVAIL. and/or SPECIAL	
A	

ACKNOWLEDGEMENT

This research was sponsored by the Space and Missile Systems Organization and the Air Force Office of Scientific Research (AFSC), United States Air Force, under Contract #F49620-78-C-0028. The United States Government is authorized to reproduce and distribute reprints for governmental purposes notwithstanding any copyright notation hereon.

TABLE OF CONTENTS

<u>Section</u>		<u>Page</u>
	Abstract	i
	Conditions of Reproduction	ii
	Acknowledgement	iii
I.	Introduction	1
II.	Rough Wall Turbulence Model	3
III.	Comparisons with Experiments on Roughness Character	6
IV.	Roughness Character Scaling Laws	26
V.	Comparisons with Experiments at High Mach Numbers	31
VI.	Summary	38
	References	40
	Appendix	42

LIST OF FIGURES

<u>Figure</u>		<u>Page</u>
1.	Computed and measured skin friction coefficients vs. distance Reynolds number, as a function of roughness spacing for spherical segments (\cong hemispheres).	8
2.	Computed mean velocity profiles compared to Schlichting measurements for spherical segments at three relative spacings.	9
3.	Computed mean velocity profiles for spherical segment roughness in classic "sand-grain" coordinates.	10
4.	Comparison of calculated roughness augmentation of skin friction vs. Schlichting measurements, for spherical roughness elements.	12
5.	Comparison of calculated skin friction augmentation vs. Schlichting experimental results, as a function of roughness spacing for three types of elements.	13
6.	Heat transfer coefficient comparison for smooth and grit blasted surfaces - 45° cones at $M \cong 7$.	16
7.	Comparison of present theory with Aerotherm data on bonded grit surface.	17
8.	Comparison with Aerotherm data on chemically etched 4 mil (nominal) roughness, close and wide spacing.	18
9.	Comparison with Aerotherm data on chemically etched 10 mil (nominal) roughness, close and wide spacing.	19
10.	Comparison of present theory with Aerotherm skin friction data, for smooth, grit blasted, and bonded grit surfaces.	21
11.	Comparison of present theory with Aerotherm skin friction data for 4 mil (nominal) chemically etched roughness.	22
12.	Comparison of present theory with Aerotherm skin friction data on 10 mil (nominal) chemically etched surfaces.	23
13.	Comparison of present theory with Holden's data for smooth and rough (4 mil bonded grit) surface.	24

LIST OF FIGURES (CONT.)

<u>Figure</u>		<u>Page</u>
14.	Skin friction vs. projected roughness area per unit surface area, according to Schlichting's data.	28
15.	Preliminary correlation of roughness "plateau" velocity versus roughness spacing at $Re = 10^4$.	29
16.	Comparison with present theory with Keel's measurements at $M_e = 4.8$ with $k = 23$ and 43 mils.	32
17.	Comparison of present theory with Keel's heat transfer data - $M_e = 4.8$, $k = 23$ and 43 mils.	33
18.	Computed boundary layer Mach number profile for $M_e = 4.8$, $k = 23$ mils.	35
19.	Comparison of present theory with Voisinet data on combined effect of roughness and mass addition.	37

LIST OF TABLES

<u>Table</u>		<u>Page</u>
I.	Schlichting Roughness Experiments	7
II.	Roughness Characteristics for Acurex AEDC Tests at Mach 7	15

I. INTRODUCTION

Surface roughness plays an important role in turbulent boundary layer skin friction and heat transfer for many high-speed flight applications. Although the general nature of roughness effects for typical types of "sand grain" roughness has been known for many years, dating back to the classic study by Nikuradse,¹ modern composite materials introduce a different character of roughness. By roughness character, we mean the shape, spacing and perhaps the distribution of roughness heights. With a woven composite material, for example, the exposed fibers would be approximately cylindrical in shape, in contrast to the more nearly hemispherical or pyramidal shape of conventional roughness elements.

Previous studies of roughness character have been somewhat limited experimentally, and the only theoretical investigations have been quite empirical. Schlichting² measured the drag due to various element shapes (spheres, spherical segments, cones) at several relative spacings on the side wall of a water channel. There are several reported experiments involving two-dimensional roughness elements (machined grooves normal to the flow direction). Some years ago, Bettermann³ correlated the available data to obtain k_s/k , the ratio of the effective sand grain roughness height to the actual roughness height, as a function of roughness shape and spacing. Of course, the effective sand grain roughness can be used in Nikuradse's results to predict the skin friction increase. Dvorak⁴ has applied Betterman's data to practical heating applications. Unfortunately, much of the data that had previously been correlated were obtained on two-dimensional roughness patterns. One might expect a difference in the nature of the flow over 2-D versus 3-D roughness. For example, with 2-D roughness, the flow could be more likely to separate, resulting in a cavity flow in the grooves between the elements. The three-dimensional case is of far greater practical importance, and the 2-D type of roughness will not be considered further here.

In this study we employ a Reynolds stress turbulent boundary layer model which specifically accounts for roughness effects. Roughness is represented by distributed sources and sinks in the various governing equations. The most important term is a sink term in the mean momentum equation representing form drag on the roughness elements. In previous studies,⁵ the approach was developed and compared against subsonic rough wall boundary layer measurements. The present objective is to apply the theory to variations in roughness character, as well as to supersonic conditions. A model extension to treat closely packed roughness elements will be described. Calculations will be compared with the Schlichting² data, as well as some recent supersonic tests on different roughness types performed in AEDC Tunnel F by Acurex Corp. Also, other available measurements on high Mach number rough wall boundary layers will be analyzed, and the nature of the roughness influence will be discussed in some detail.

II. ROUGH WALL TURBULENCE MODEL

The turbulence model used here is one in which closure approximations are applied at second order. With the exception of the treatment of roughness, the formulation is somewhat standard at this time, and has been successfully applied to a variety of smooth wall boundary layer and free shear flows. The model accounts for both mean and fluctuating velocities and temperatures. The dependent velocity variables are the mean velocity vector U_i , the Reynolds stress tensor $\overline{u_i' u_j'}$, and the isotropic dissipation rate ϕ . The analogous thermal variables (temperature or, more precisely, enthalpy h) are the mean enthalpy \bar{h} , the mean square fluctuating enthalpy h'^2 , and the Reynolds heat flux vector $\overline{u_i' h'}$. Under the boundary layer approximation, this set of variables reduces to U , v , u'^2 , v'^2 , w'^2 , $u'v'$, ϕ , \bar{h} , h'^2 , $u'h'$, and $v'h'$. The development of the governing equations and the required closure approximations were described in Ref. 5 and will not be repeated here. The actual equations are given in the Appendix.

The effect of roughness is described by distributed source or sink terms in the appropriate equations. As already noted, only distributed roughness is considered here, and we make the fundamental assumption that the flow around individual elements is attached to the elements. For two-dimensional roughness, the flow might be treated more appropriately as cavity flows between the elements. In the present model, roughness elements provide a distributed sink (due to drag) for mean momentum, and distributed sources for mean turbulent kinetic energy and dissipation. We idealize the rough surface as being made up of identical elements (although the extension to a size distribution is feasible). The bottom of the elements corresponds to $y = 0$. Let k be the element height, $D(y)$ be the element diameter by height y (for $0 \leq y \leq k$), and λ be the average center-to-center element spacing. The functional form of the diameter $D(y)$ is easily prescribed for simple shapes such as cones or hemispheres. As discussed in Ref. 5 and in the Appendix, the drag on the elements per unit volume is the appropriate sink term in the equation for the mean velocity:

$$R_u = - \frac{1}{2} \rho U^2 C_D D(y)/\ell^2 . \quad (1)$$

A drag coefficient value of $C_D = 0.5$ is roughly appropriate for elements such as cones or hemispheres. The source terms for kinetic energy and dissipation, which are less important numerically, are given in the Appendix. Except in the Stokes flow regime, heat transfer to an element should be small. Therefore, the only roughness term appearing in the thermal equations is a source for the mean enthalpy. This term is simply constructed so that, in combination with Eq. (1), form drag does not alter total enthalpy:

$$R_h = + \frac{1}{2} \rho U^3 C_D D(y)/\ell^2 . \quad (2)$$

In the approach that we have just outlined, roughness elements are assumed to occupy no physical space. This assumption becomes progressively worse as the roughness density increases. Accordingly, the model has been extended to account for the blockage effect of the roughness elements. This is done in a quite simple manner. At a given height y , the fraction of the flow area in the x direction, that is open to the flow, is $1 - D(y)/\ell$; terms that act in the streamwise direction, such as the convective operator $\rho u \partial/\partial x$, are multiplied by this factor. Terms that act on a surface area whose normal is in the y direction, or that act on a unit volume, should be multiplied by $1 - \pi D^2/4\ell^2$. However, the distributed roughness source or sink terms are already based on the total volume, rather than available flow volume, and need no such factor. If the entire equations are divided by $1 - \pi D^2/4\ell^2$, a relatively simple change occurs. For example, the mean momentum equation becomes

$$\begin{aligned} f(y) \rho U \frac{\partial U}{\partial x} + \rho v \frac{\partial U}{\partial y} = & - f(y) \frac{\partial p}{\partial x} + \frac{\partial}{\partial y} \left(\mu \frac{\partial U}{\partial y} \right) \\ & - \frac{\partial}{\partial y} (\rho \overline{u'v'}) - \frac{1}{2} \rho U^2 C_D \frac{D}{\ell^2} \left(1 - \frac{\pi D^2}{4\ell^2} \right)^{-1} \end{aligned} \quad (3)$$

where

$$f(y) = \frac{1 - D/\ell}{1 - \pi D^2/4\ell^2} \quad (4)$$

The function $f(y)$ may be handled by merely redefining the standard stream function which is used to eliminate the normal velocity.

$$\frac{\partial \phi}{\partial y} = f(y)\rho U, \quad \frac{\partial \phi}{\partial x} = -\rho V. \quad (5)$$

Note that if the elements are packed so tightly that they are touching over some range of y , then $D = \ell$ and $f(y) = 0$. The stream function would be forced to be independent of y over that range (from Eq. (5)); the velocity would remain zero from the bottom of the elements up to the height where $D < \ell$ and flow is unblocked. Of course, common sense would dictate redefining $y = 0$ as the lowest point where the flow is unblocked. However, the model does yield the limiting result that $U = 0$ if there is no space between the elements.

A major advantage of the PSI Reynolds stress model is that solutions are obtained for both velocity and thermal variables. Heat transfer is obtained directly, without invoking a Reynolds analogy. Finite difference solutions are obtained using the obvious boundary conditions: fluctuating quantities are zero at the solid wall and in the free stream. It is important to note that the boundary conditions at the wall are not treated as empirical functions of roughness as has been done in other approaches.⁶ For numerical solutions, the equations are first transformed to the stream function coordinate, guaranteeing continuity and eliminating the normal velocity V . The transverse coordinate is normalized by the edge value of the stream function, so that additional mesh points need not be carried in the free stream to allow for boundary layer growth. For proper resolution of the region near the wall, a linear mesh in the logarithm of the stream function is used. The finite-difference equations are solved with a block tridiagonal Newton-Raphson technique.

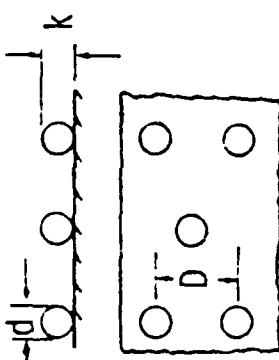
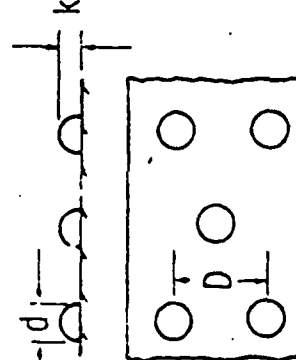
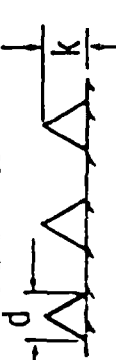
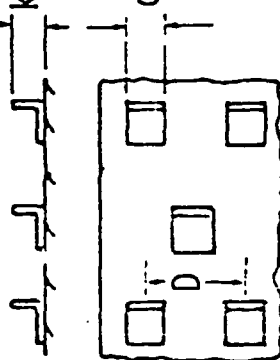
III. COMPARISONS WITH EXPERIMENTS ON ROUGHNESS CHARACTER

The first measurements to be examined are those of Schlichting, which were obtained in a 4 cm x 17 cm water channel. Various arrangements of roughness elements, shown in Table I, were used on the top wall. Velocity profiles were measured, and the skin friction or equivalent sand grain roughness k_s was derived from the logarithmic portion of the profile. The simple shapes and regular spacing of the roughness elements can be simulated quite well by our roughness model, with the exception of the short angles, which were not investigated.

Figure 1 compares the skin friction computed with our model against Schlichting's data for the spherical segments. As indicated in Table I, the segments are nearly hemispherical (height = 0.26 cm, radius = 0.40 cm). Further, the dashed lines were not actually presented by Schlichting.² He determined the equivalent sand grain roughness, based on the observed increase in C_f over the smooth wall value, at selected downstream stations. We took the liberty of using the k_s values to obtain the augmentation of C_f as a function of distance. In so doing, the appropriate upstream initial conditions are ignored. The computations were started with a fully turbulent smooth wall boundary layer at $x/l = 0.03$. Given the arbitrary treatment of initial conditions, the mild disagreement at upstream locations is not significant. Otherwise, the model reproduces fairly well the observed increase in skin friction with increasing roughness density.

A detailed comparison of the mean velocity profiles computed from the PSI model with Schlichting's data is shown in Fig. 2, in semi-logarithmic coordinates ($U_T = \sqrt{\tau_w/\rho_w}$). Agreement is again seen to be quite good, with a 10-15% error for the most dense packing. Figure 3 replots the same results, normalized by the equivalent sand grain roughness; the similarity expected from classic rough wall pipe flow is evident. One interesting point of the calculation for the case with $l/D = 2.5$ is that the computed velocity is nearly constant over a significant range of heights up to almost the top of the elements (which is at $y/k_s = 1.75$ for this case). This behavior will be discussed in more detail in Section IV.

TABLE I. SCHLICHTING ROUGHNESS EXPERIMENTS

Roughness Elements	Dimension	D cm	d cm	k cm	k _s cm	Measurement		
Schlichting	 <p>Diagram showing a surface with spherical roughness elements. A side view shows a sphere of diameter d with a height k. A top view shows a rectangular plate with four spheres, each with diameter D.</p>	4	.41	.41	.093	Velocity Profiles- C_f		
		2	.41	.41	.344			
		1	.41	.41	1.26			
		.6	.41	.41	1.56			
		1	.21	.21	.172			
		.5	.21	.21	.759			
	Spherical Segments	 <p>Diagram showing a surface with spherical segment roughness elements. A side view shows a segment of height k and diameter d. A top view shows a rectangular plate with four segments, each with diameter D.</p>	4	0.8	0.26	.031		
			3	0.8	0.26	.049		
			2	0.8	0.26	.149		
			Cones	 <p>Diagram showing a surface with conical roughness elements. A side view shows a cone of height k and diameter d. A top view shows a rectangular plate with four cones, each with diameter D.</p>	4	0.8	.375	.059
					3	0.8	.375	.164
					2	0.8	.375	.374
Short-angles	 <p>Diagram showing a surface with short-angled roughness elements. A side view shows a short-angled element of height k and diameter d. A top view shows a rectangular plate with four elements, each with diameter D.</p>	4	0.8	0.30	.291			
		3	0.8	0.30	.618			
		2	0.8	0.30	1.47			

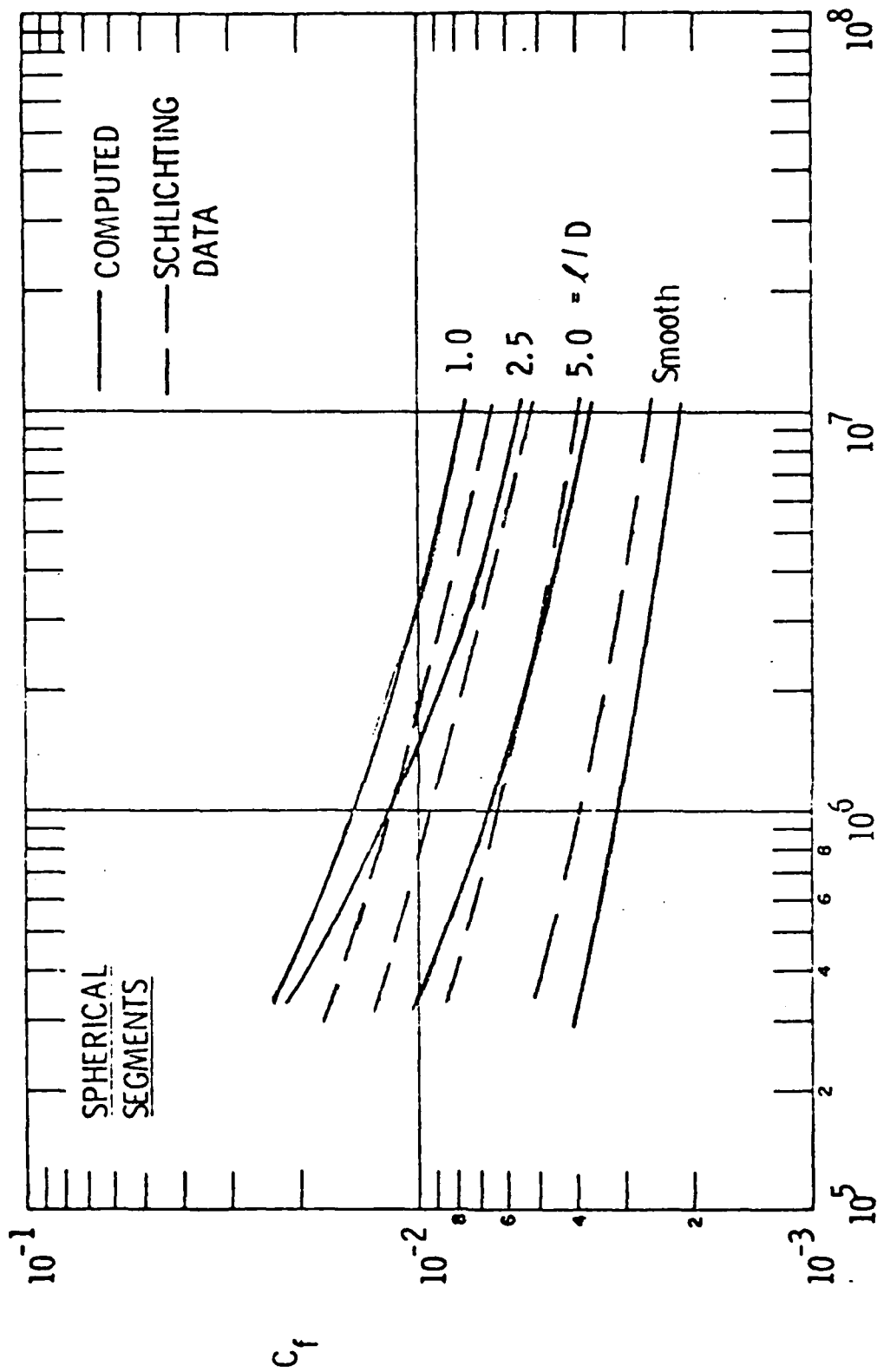


Fig. 1 - Computed and measured skin friction coefficients vs distance Reynolds number, as a function of roughness spacing for spherical segments (\approx hemispheres).

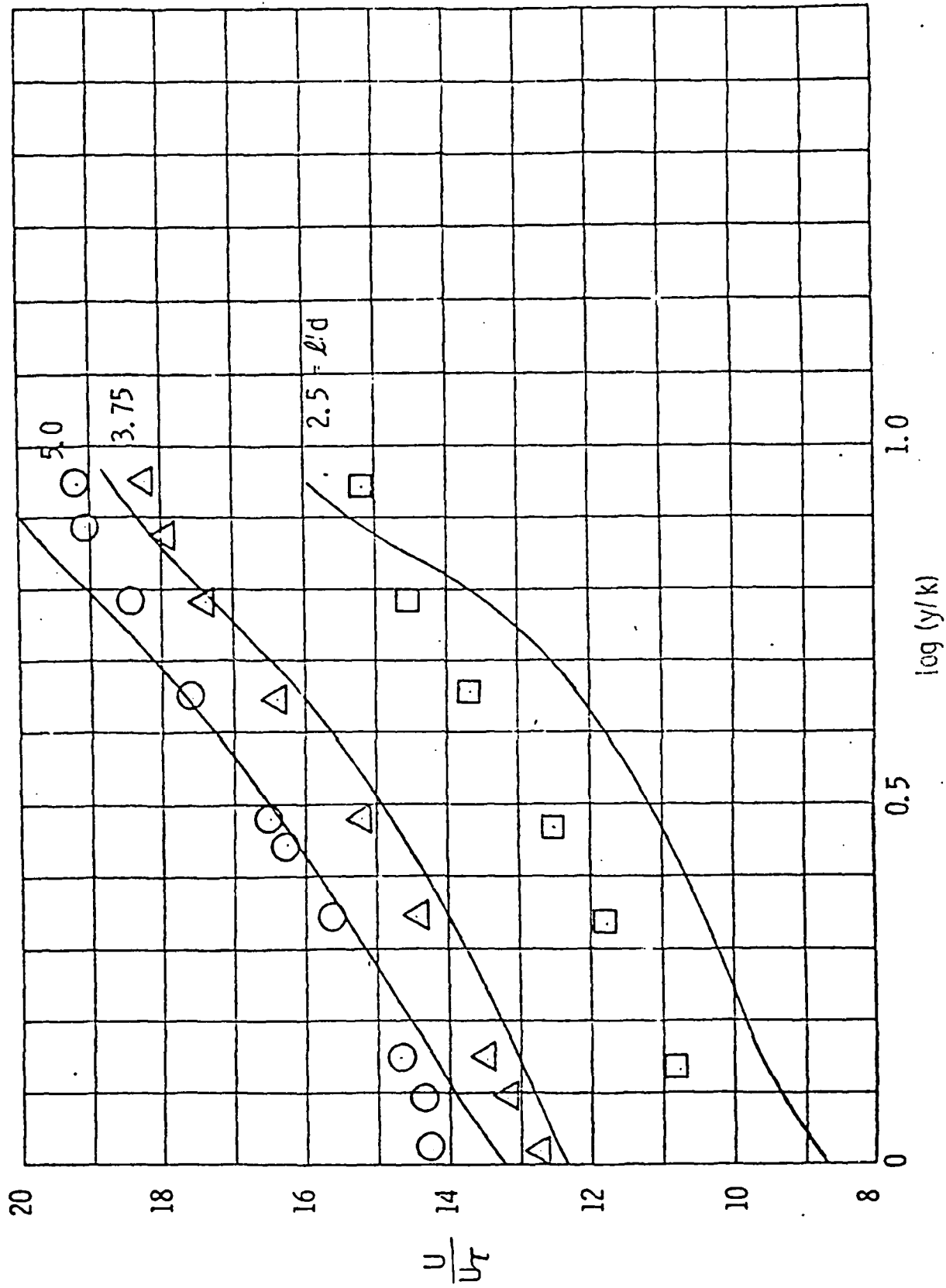


Fig. 2 Computed mean velocity profiles compared to Schlichting² measurements for spherical segments at three relative spacings.

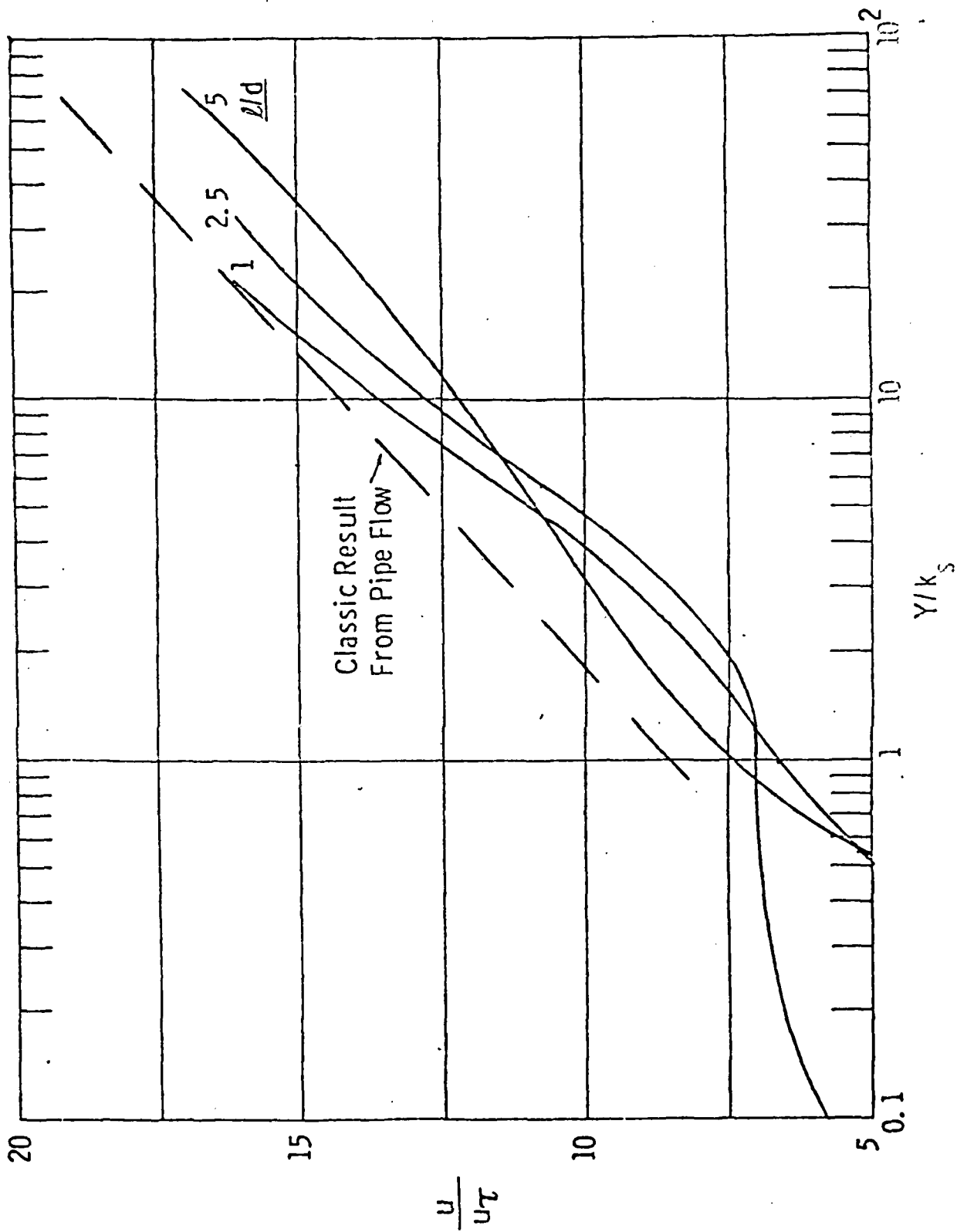


Fig. 3 Computed mean velocity profiles for spherical segment roughness in classic "sand-grain" coordinates.

Figure 4 shows the computed skin friction coefficients and Schlichting's measurements for spherical elements as a function of spacing. The calculations were evaluated at $Re_x \approx 10^7$, but the increase in skin friction is essentially independent of distance. The decrease in C_f as $l/D \rightarrow 1$ is easy to explain qualitatively. At large l/D the flow "sees" the entire sphere. With substantial element spacing, the drag increases with decreasing l/D because there are more elements per unit area. But as $l/D \rightarrow 1$ the flow becomes negligible below the centers of the spheres and the drag is due only to the upper half of the elements.

The corresponding plot for spherical, spherical segment, and conical roughness elements is shown in Fig. 5. The spherical comparison is omitted for $l/D < 2$; the cones and segments were not investigated at such close spacings. The calculations for the cones and segments are almost identical (although the cones are slightly taller, 0.375 cm vs 0.26 cm). However, the data for the cones fall above that for the segments. This implies that the effective drag coefficient for the flow about a conical roughness element is somewhat larger than that for flow about spherical elements. The same value was used in all of our calculations. If one were to allow such a higher value of C_D for cones, the influence of roughness element shape would be well understood.

The second set of interesting tests was carried out by Acurex Corporation in AEDC Tunnel F,⁷ using 45° conical models with a variety of surface roughnesses. This facility was an arc-driven hot shot tunnel, in which the test section pressure decreased during the run (total time ≈ 200 msec). The most useful tests were performed on sharp 45° cones at $M_\infty \approx 7$ at a free stream Reynolds number of 45×10^6 /ft. N_2 was the test gas. The first 0.75" of wetted length was roughened to 4-5 mils to ensure rapid transition.

Seven surface finishes were used on the remainder of the cones; essentially smooth, grit blasted to almost 2 mils, 2 mil bonded grit, and four chemically-etched roughness patterns (wide and close spacing at nominal heights of 4 and 10 mils). The etching process resulted in roughness elements that were best approximated as truncated cones (top

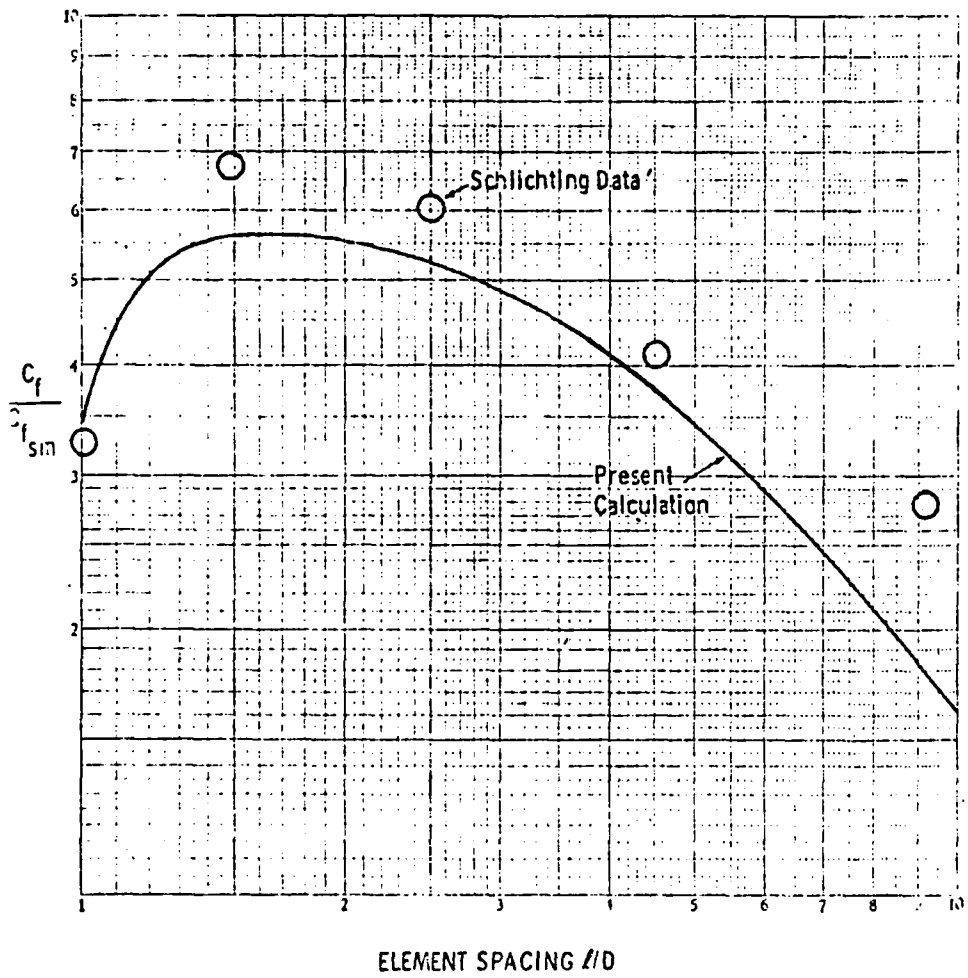


Fig. 4. Comparison of calculated roughness augmentation of skin friction vs. Schlichting measurements, for spherical roughness elements.

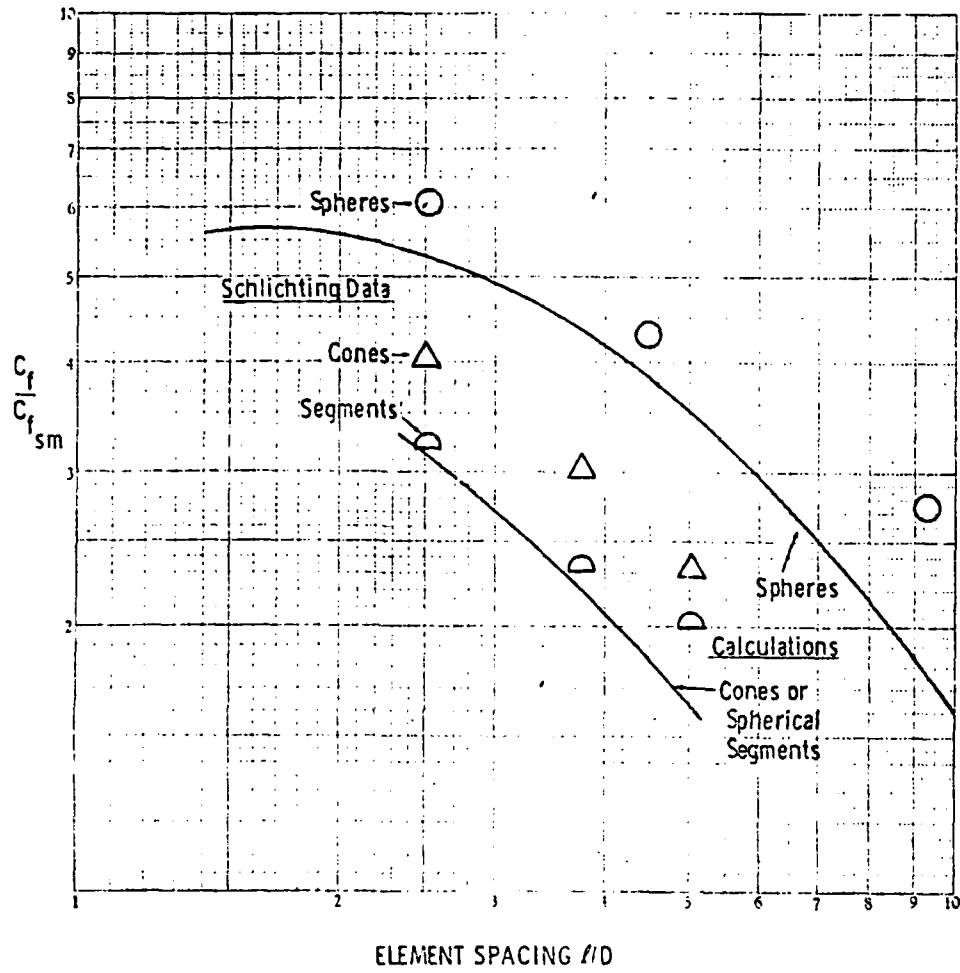


Fig. 5. Comparison of calculated skin friction augmentation vs. Schlichting experimental results, as a function of roughness spacing for three types of elements.

radius $\approx 1/4$ base radius) whereas the grit roughness elements are simulated with hemispheres. The roughness characteristics of these chemically milled surfaces varied by as much as $\pm 30\%$ in mean roughness height over the surface of the cones. Table II lists the average element height and spacing for the various surfaces. Note that the "4 mil" etched roughness is actually considerably less rough. Also, the "4 mil" roughnesses have larger relative roughness spacing than the "10 mil" surfaces. In fact, the "4 mil close" and "10 mil wide" roughnesses have essentially the same ℓ/k .

The primary measurements for this test series are the heat transfer rates, determined by thin wall calorimetry with thermocouples on the back wall. Some co-axial heat transfer gauges, as well as skin friction gauges, were also used, although there may be uncertainties regarding how faithfully the roughness is reproduced on the surface of the gauges. Figures 6 through 9 compare the Stanton numbers, $q/\rho_e u_e C_p (T_r - T_w)$, calculated by the present model with the Acurex data.

The agreement is seen to be good, with the theory generally well within the scatter of the data. Several trends are evident from either data or calculations. The bonded grit and grit blasted surfaces cause a similar heating augmentation, although the bonded grit is slightly taller and considerably more densely packed; a blockage effect must be counter-acting the more obvious effect of element spacing. However, for the chemically etched surfaces, spacing appears to be more important than height. The 10-mil wide spacing yields a greater heating rate than the 4-mil (actually 3-mil) wide case only at larger distances, and the 4-mil and 10-mil close spacing results are also quite similar. As

*The data points have actually been derived by dividing the reported heat transfer coefficients by our computed values of $\rho_e u_e$ and the specific heat of N_2 . Table II includes the values used for $\rho_e u_e$ for the various cases. Note that $\rho_e u_e$ varies by as much as 18% from one case to another, and examination of the heat transfer rate (q) rather than the Stanton number could possibly lead to inaccurate conclusions on the effect of roughness.

TABLE II. Roughness Characteristics for Acurex AEDC Tests at Mach 7

<u>Designation</u>	<u>Mean k (mils)</u>	<u>Mean Spacing l (mils)</u>	$\rho_e u_e \left(\frac{\text{kg}}{\text{m}^2 \text{sec}} \right)$
Smooth	---	---	2038
Grit Blasted	1.63	7.70	2235
Bonded Grit	2.00	4.00	2292
4 mil Wide	3.00	23.0	2157
4 mil Close	2.50	13.0	2357
10 mil Wide	10.32	56.0	1998
10 mil Close	9.50	31.0	2315

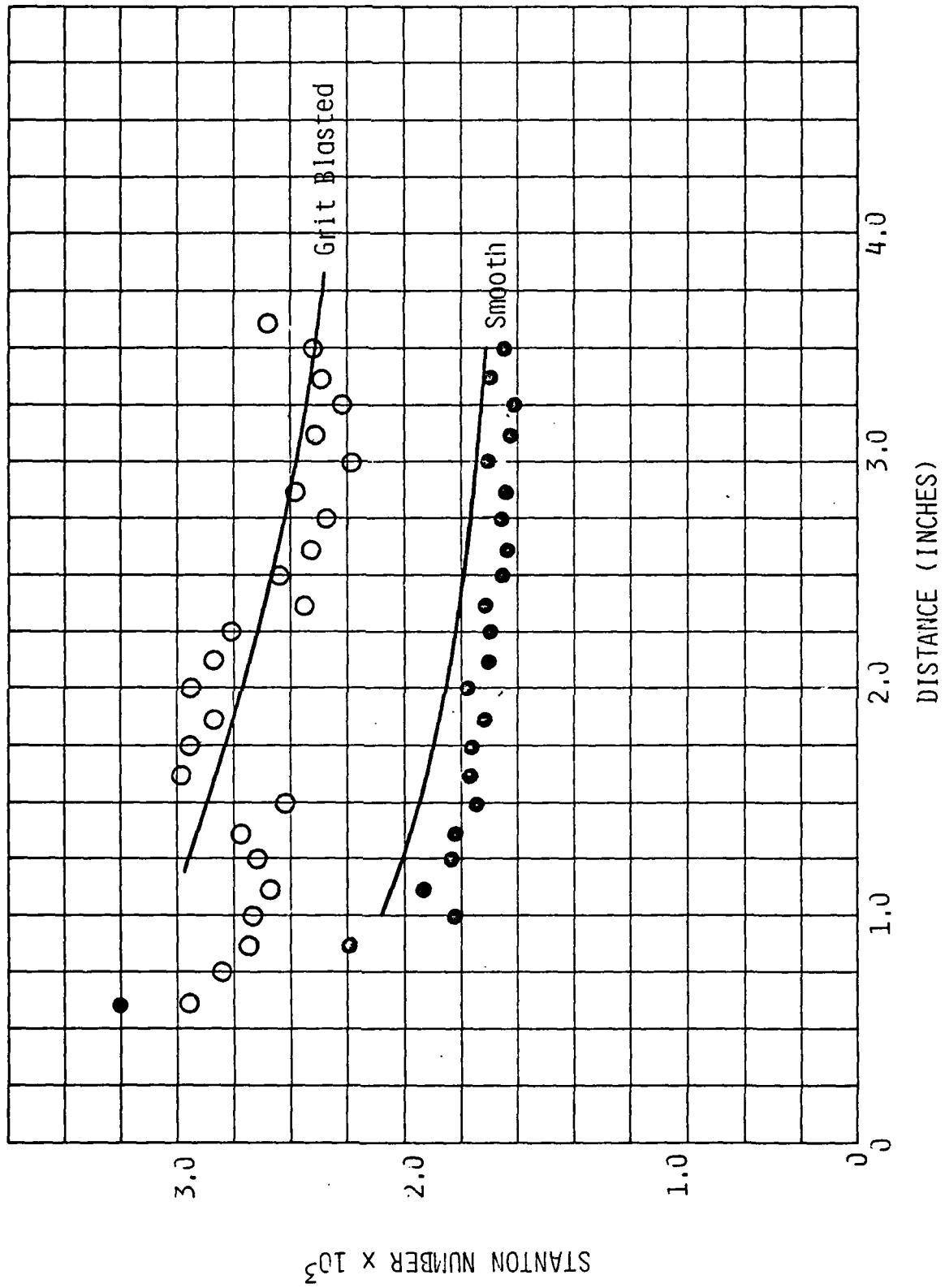


Fig. 6. Heat transfer coefficient comparison for smooth and grit blasted surfaces - 45° cones at M_∞ = 7.

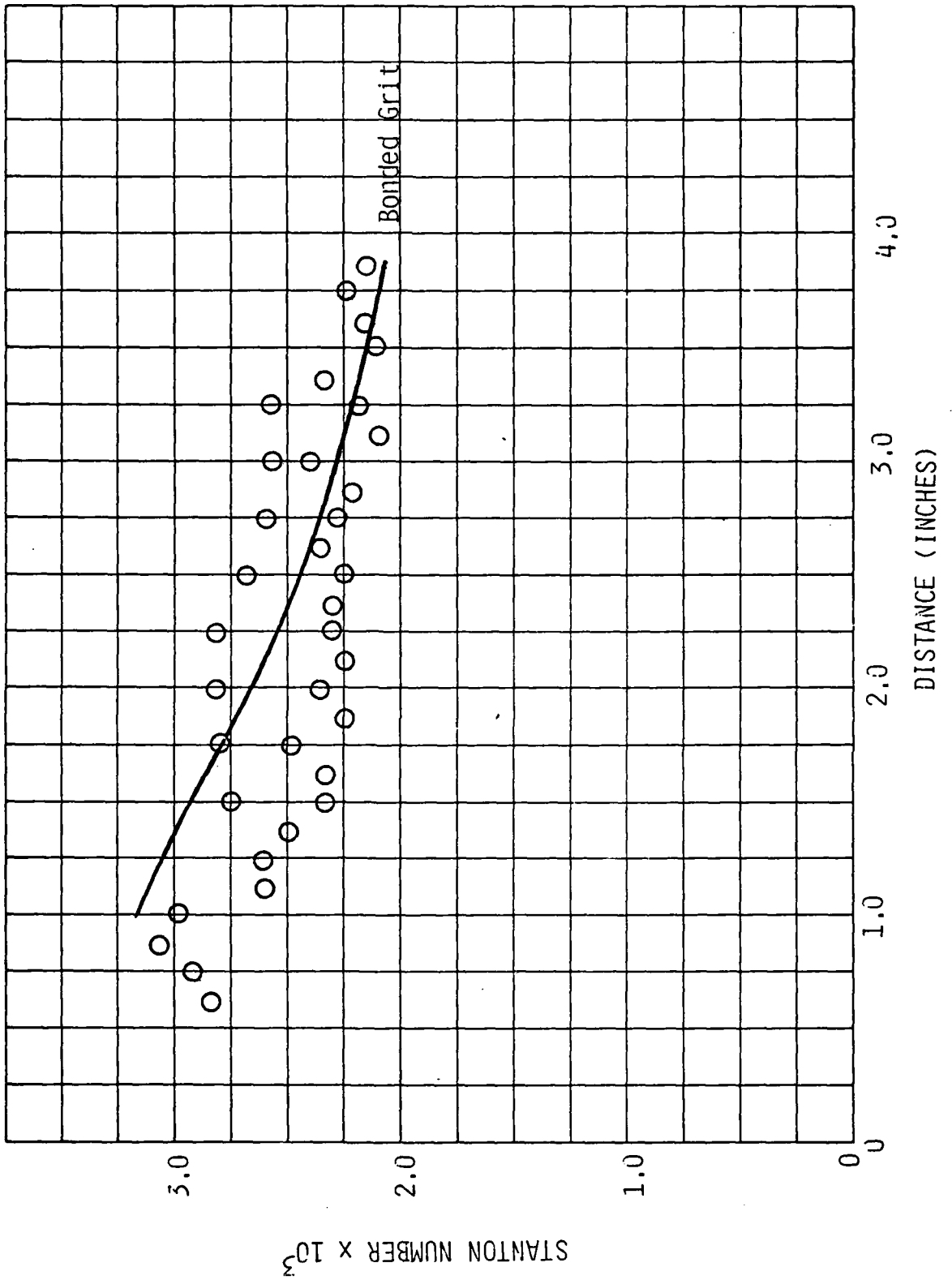
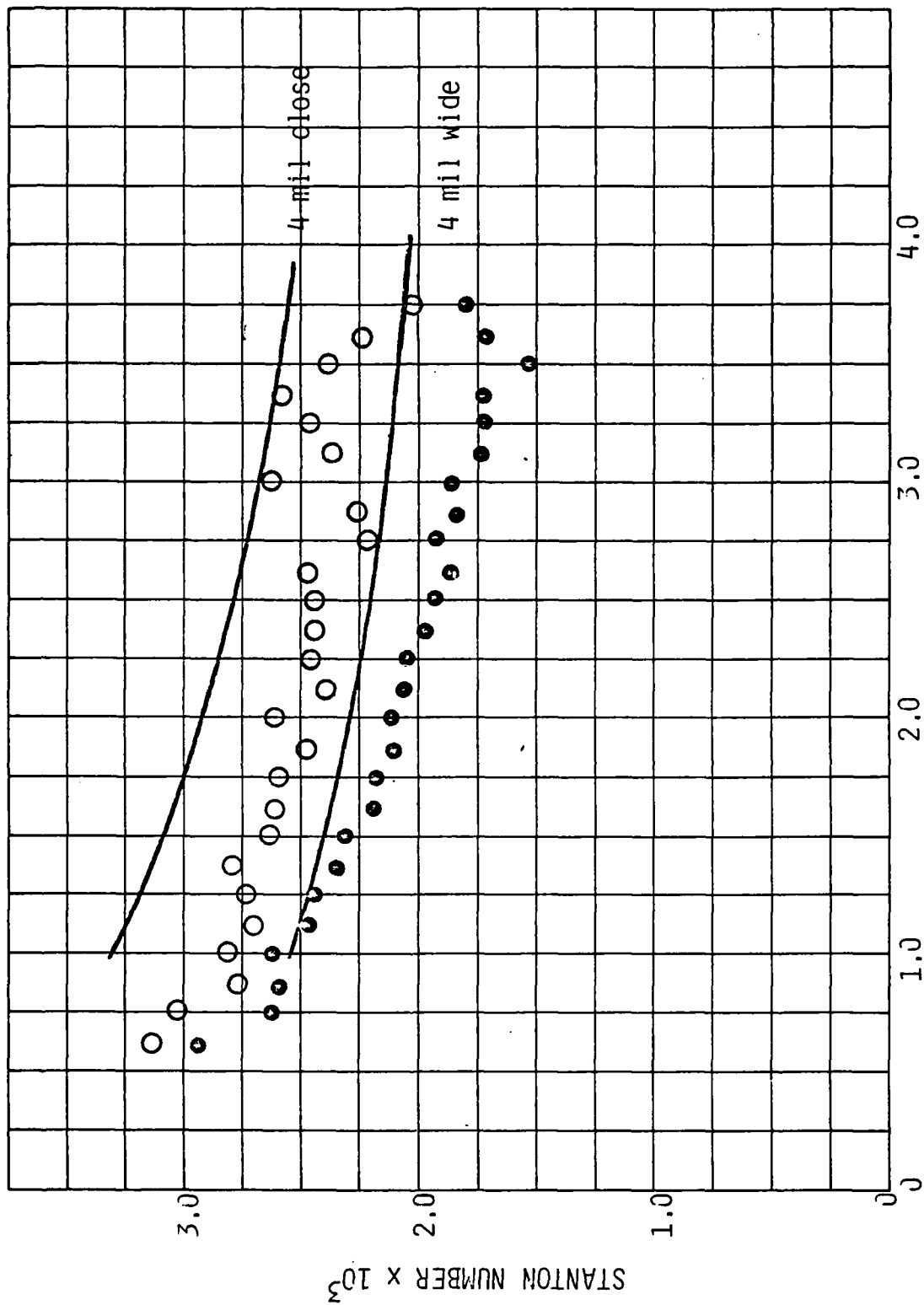


Fig. 7. Comparison of present theory with Aerotherm data on bonded grit surface.



DISTANCE (INCHES)

Fig. 8. Comparison with Aerotherm data on chemically etched 4 mil (nominal) roughness, close and wide spacing.

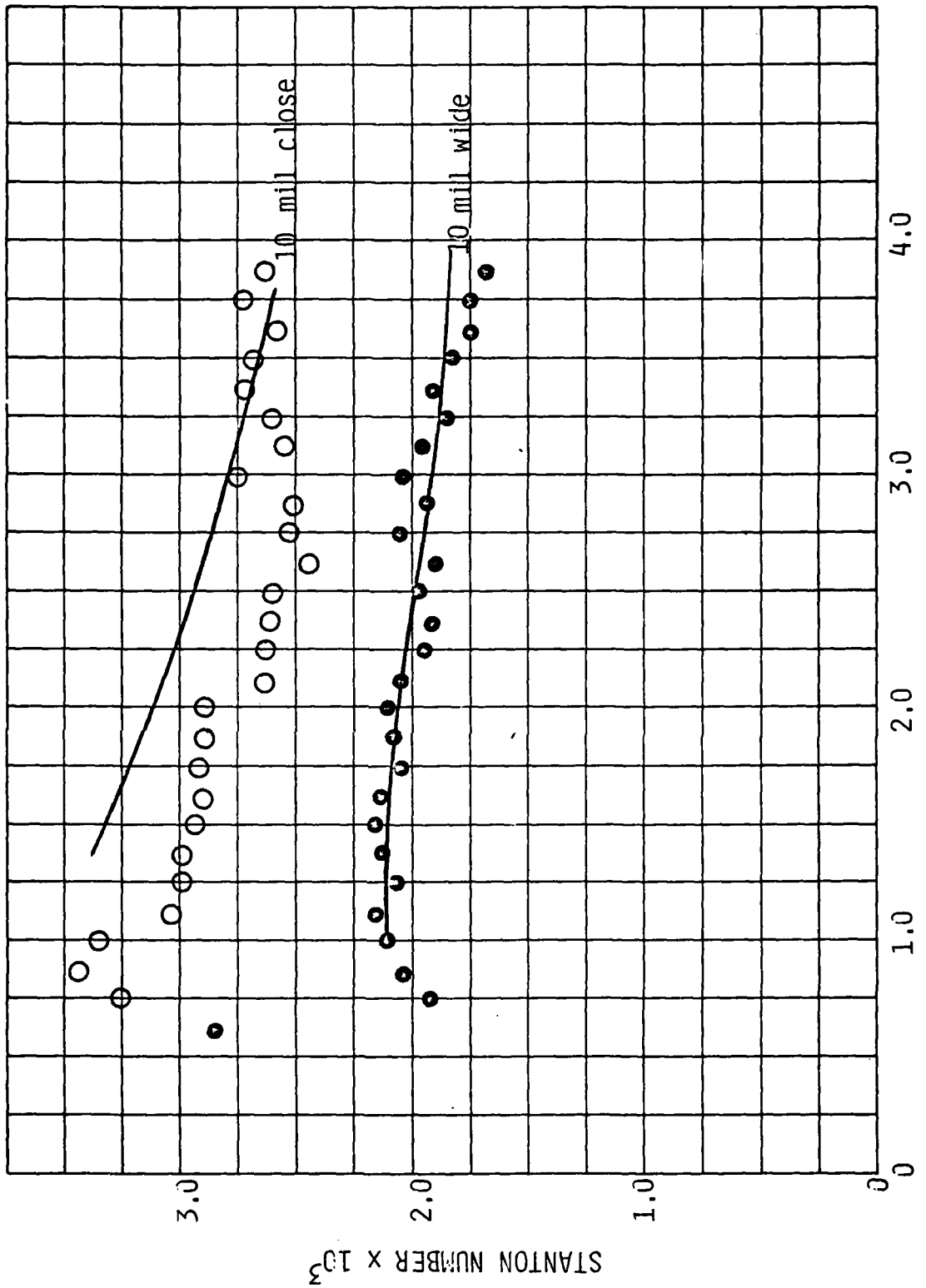


Fig. 9. Comparison with Aerotherm data on chemically etched 10 mil (nominal) roughness, close and wide spacing.

already noted, the relative roughness is not constant between the 4- and 10-mil heights, and a more detailed discussion of the dependence on height, shape and spacing is presented below.

The corresponding skin friction data are far more tentative. The floating skin friction sensors were located at only three stations, and the measurements have yet to be analyzed in any detail by the experimenters. The comparisons for the skin friction coefficients* are shown in Figs. 10 through 12. The computations exhibit much the same trends as seen for the heat transfer, although it is well known (e.g. Ref. 5) that the skin friction is augmented by larger factors than heat transfer is. Obviously, the AEDC skin friction data are highly variable. The bond grit measurements show a very pronounced decay with distance, and we can offer no interpretation for the 4-mil data of Fig. 11. Agreement with the other cases is reasonable. However, the skin friction data need to be substantiated before meaningful conclusions can be reached.

Another interesting experiment on roughness effects has been concluded in the hypersonic shock tunnel at Calspan.⁹ Only one roughness was studied - a bonded grit similar to that employed by Acurex in the series discussed above. The mean roughness height was 3.8 mils, with a spacing of 10-15 mils (we specified 12.5 mils for the spacing). As with the Acurex series, the models were 45° cones. The free stream Mach number was 11-13, although this larger value has little effect on the edge Mach number, due to the large cone angle. T_w/T_e is considerably less in the Calspan conditions. Heat transfer was measured with thin film gauges covered with the surface roughness. Figure 13 shows our comparison with Holden's results, for smooth and roughened surfaces, on a sharp 45° cone at the highest Reynolds number tested. The smooth wall boundary layer was naturally turbulent near the nose. The reported heat flux data were reduced to Stanton numbers by dividing by our computed edge value of $\rho_e u_e C_p (T_r - T_w)$, which is 6.38×10^4 BTU/ft²-sec for both

*Here again we have normalized the friction by boundary layer edge conditions, rather than by free stream conditions as originally reported.

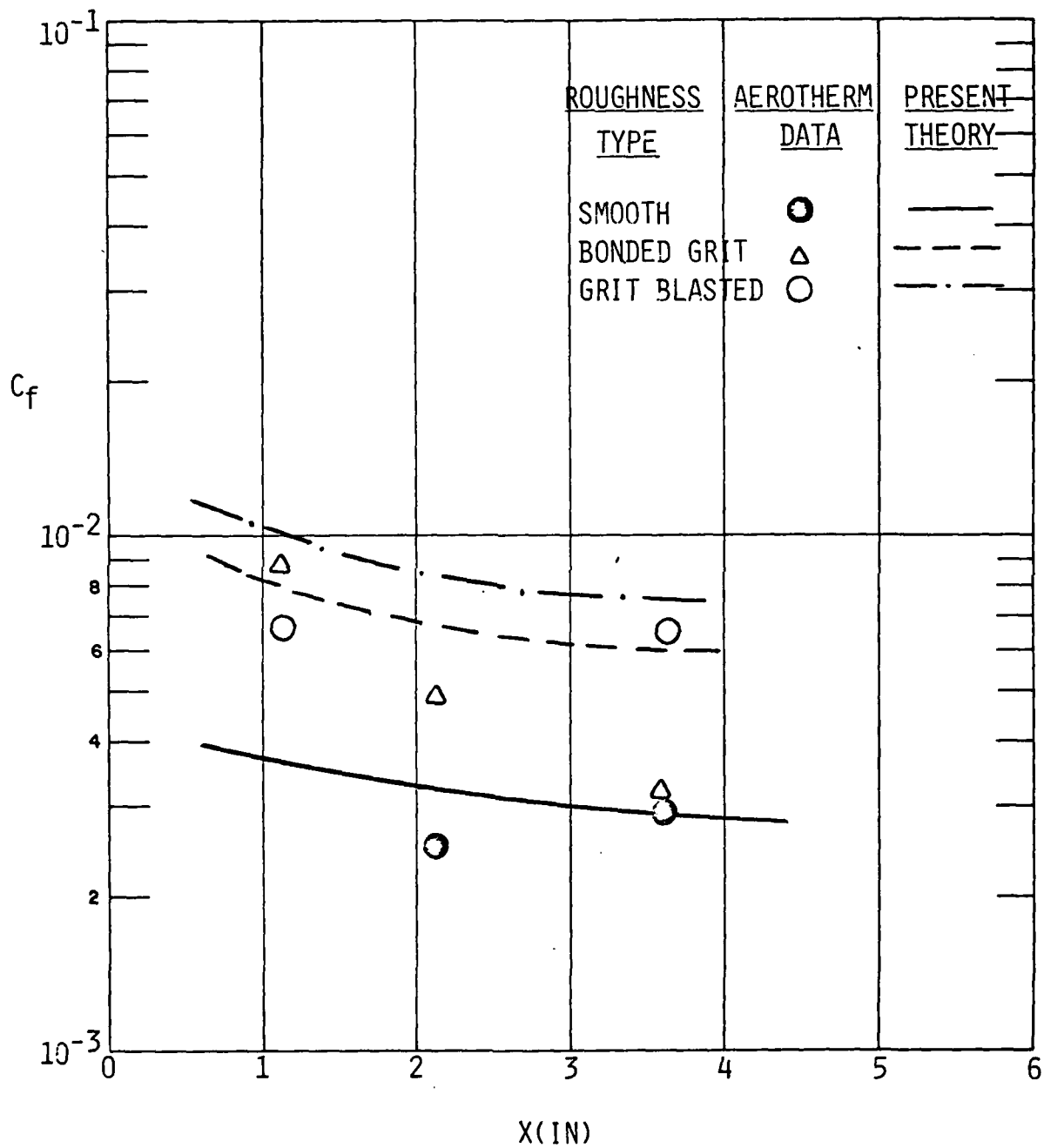


Fig. 10 Comparison of present theory with Aerotherm skin friction data, for smooth, grit blasted, and bonded grit surfaces.

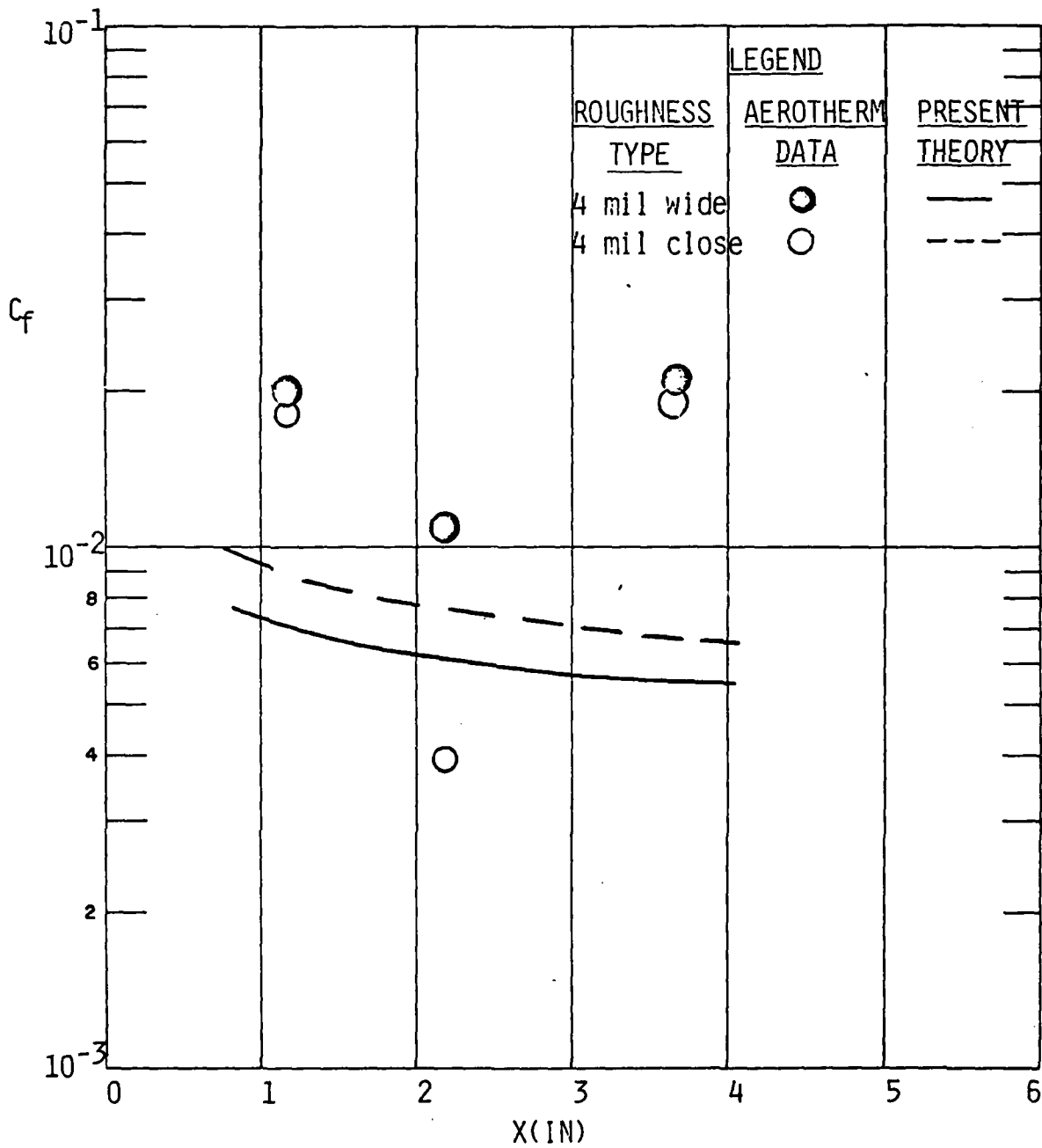


Fig. 11 Comparison of present theory with Aerotherm skin friction data for 4 mil (nominal) chemically etched roughness.

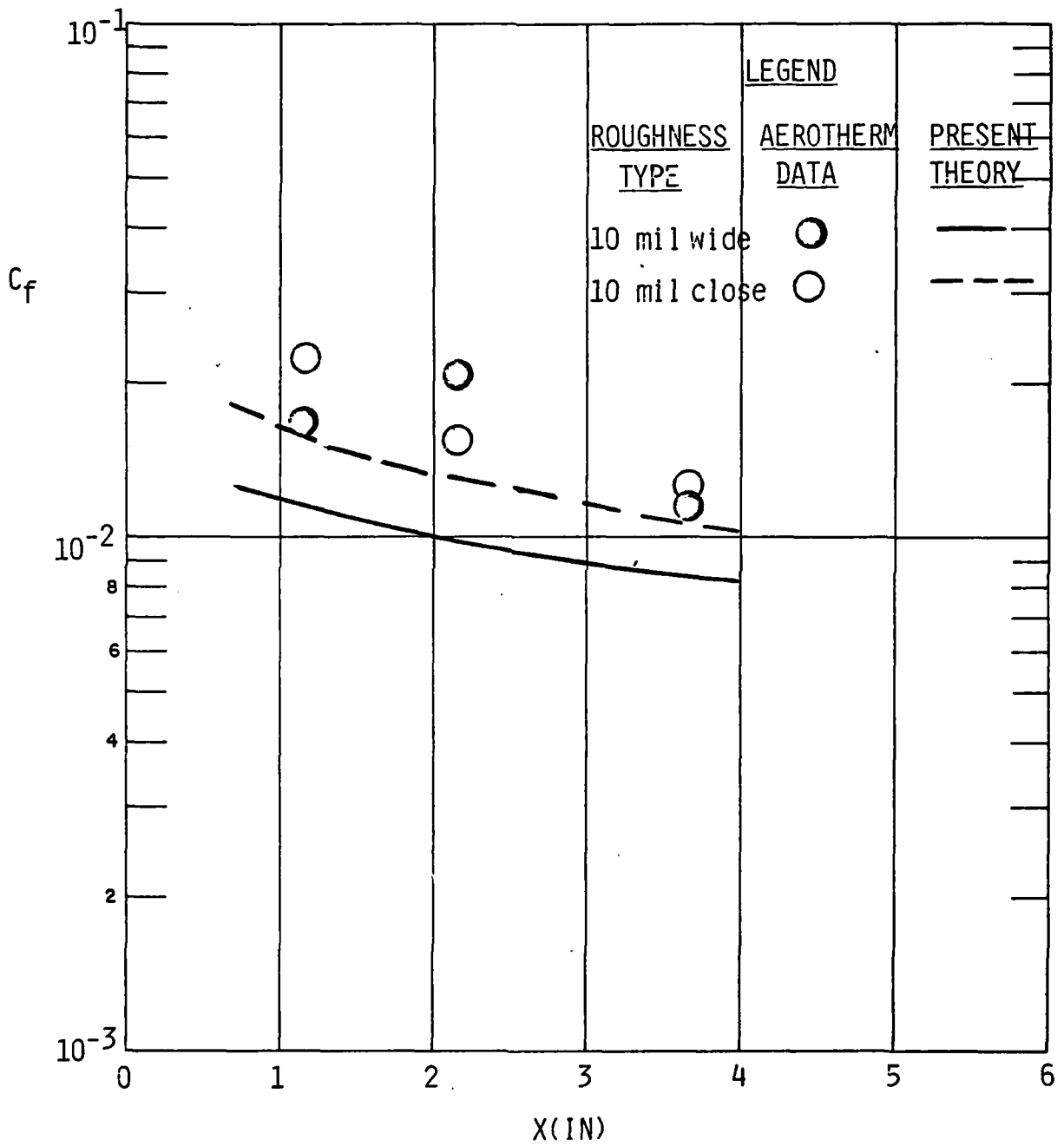


Fig. 12 Comparison of present theory with Aerotherm skin friction data on 10 mil (nominal) chemically etched surfaces.

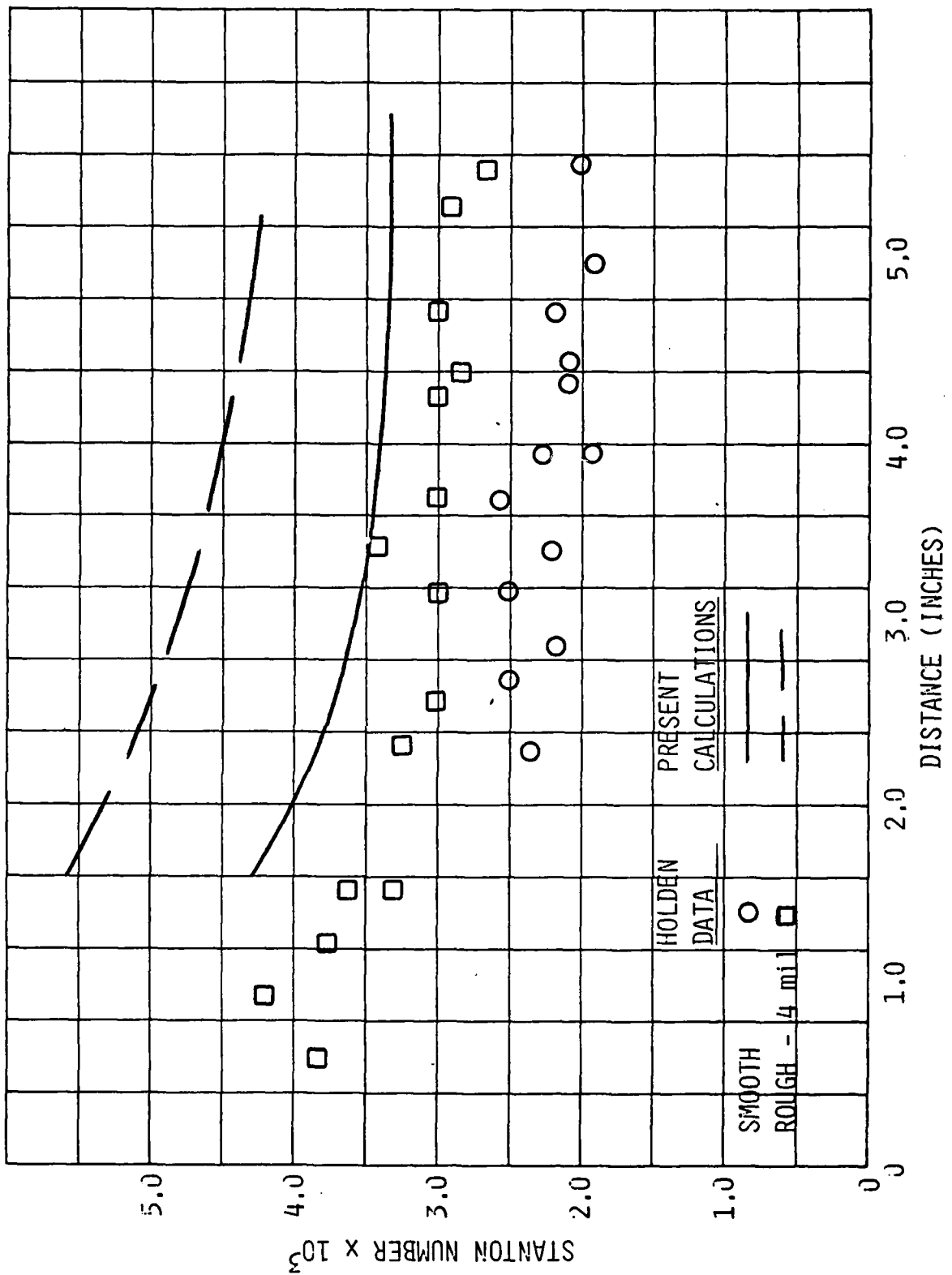


Fig. 13. Comparison of present theory with Holden's data for smooth and rough (4 mil bonded grit) surface.

smooth and rough walls. It is immediately evident that the model yields heating rates higher than measured, even for the smooth wall. The observed smooth wall Stanton number is consistent with values predicted from accepted engineering methods such as that of van Driest¹⁴ ($St \approx 2.50 \times 10^{-3}$). Although the observed roughness heating augmentation is predicted reasonably well, the discrepancies in the absolute level are bothersome and are the subject of an on-going examination. It appears that the effect is connected with the low wall temperature, which was $T_w/T_e \approx 0.34$ in contrast to the Acurex series where $T_w/T_e \approx 0.75$. The large resulting density variation across the boundary layer seems to cause inaccuracy either in the numerical techniques or closure approximations. The present results have been substantiated by increasing the computational mesh spacing in both the x and y directions. However, the issue remains open, and may be unique to relatively low edge Mach number, low T_w/T_e conditions.

IV. ROUGHNESS CHARACTER SCALING LAWS

While the PSI rough wall boundary layer theory reproduces the available measurements on the effect of roughness character variations, the theory is not readily useful for flight vehicle design and analysis. The finite difference solution of the coupled Reynolds stress equations is too cumbersome to be incorporated into current RV nosetip shape change codes, for example, although our methods require efforts that are at least 2 to 3 orders of magnitude less than those involved in present state-of-the-art computational fluid dynamic methods. Relatively simple scaling laws for the dependence of roughness augmentation on element shape and spacing are needed. The model results presented here can be examined to determine the nature of roughness-induced flow changes, leading to physically well-founded correlations. In this section we shall present a progress report on determining the nature of roughness character effects, although the ultimate scaling laws have yet to be derived.

The keystone to understanding the nature of roughness effects on turbulent boundary layers is the fact that our computer solutions indicate the mean velocity to be quite uniform over much of the range $y \leq k$. An example of this behavior was noted in Fig. 3 above, for $\ell/d = 2.5$. The top of the elements is at $y/k_s = 1.75$ for this case, and the velocity exhibits a "plateau" at $u/u_T \approx 7$ or $u/u_e \approx 0.38$. For the other two spacings shown there, the plateau covers a smaller range in y and lies off the scale of the figure, at $u/u_T < 5$. Of course, the mean velocity cannot be strictly constant for $y < k$. Very near the wall (i.e., at the bottom of the elements) the velocity must be zero, and near the tops of the elements, the velocity tends to increase. The velocity plateau, which was unexpected, is evident in almost all of the cases considered, the sole exceptions being cases with very small roughness (say $k^+ \lesssim 10$ where $k^+ = \rho_w u_T k / \mu_w$) or very large roughness ($k/\theta > 1$).

If the mean velocity is nearly constant over the range $y < k$, then the momentum equation reduces to

$$0 \cong - \frac{\partial}{\partial y} (\rho \overline{u'v'}) - \frac{1}{2} \rho U^2 C_D \frac{D(y)}{\ell^2} . \quad (6)$$

The total form drag on the elements, which should be close to the actual skin friction, is easily related to the element shape

$$C_f \sim \int_0^k \frac{\rho U^2}{\rho_e U_e^2} C_D \frac{D(y)}{\ell^2} dy \cong \frac{\rho_w U_p^2}{\rho_e U_e^2} C_D \int_0^k \frac{D(y)}{\ell^2} dy . \quad (7)$$

The final integral is the frontal area of the elements per unit superficial surface area. The value of the plateau velocity U_p will depend on roughness parameters, as will be discussed. A partial correlation is given by plotting the observed skin friction against this ratio of projected element area per unit surface area. This is done in Fig. 14 for the Schlichting data, omitting the cases with $\ell/D = 1$. A reasonable correlation is apparent, although C_f increases with projected element area at less than the linear rate suggested by Eq. 7.

The value of the plateau velocity is the other important part of roughness scaling behavior. In Fig. 15 we show an empirical attempt to describe this velocity. The values have been obtained from our computer solutions without attempting to be particularly objective in the manner by which the values were selected. Examination of the results shows no organized trend in terms of roughness height or k^+ ; the correlation against relative spacing is not perfect, but does reflect the trend for more closely packed elements to reduce the velocity between the elements.

A proper means for predicting the plateau velocity U_p should be derivable from a simplified analysis of the Reynolds stress model used in this study. In Eq. 6 above it was shown that the mean momentum equation simplifies greatly for $y < k$. Examination of typical sets of output profiles indicates that the various Reynolds stress equations also simplify

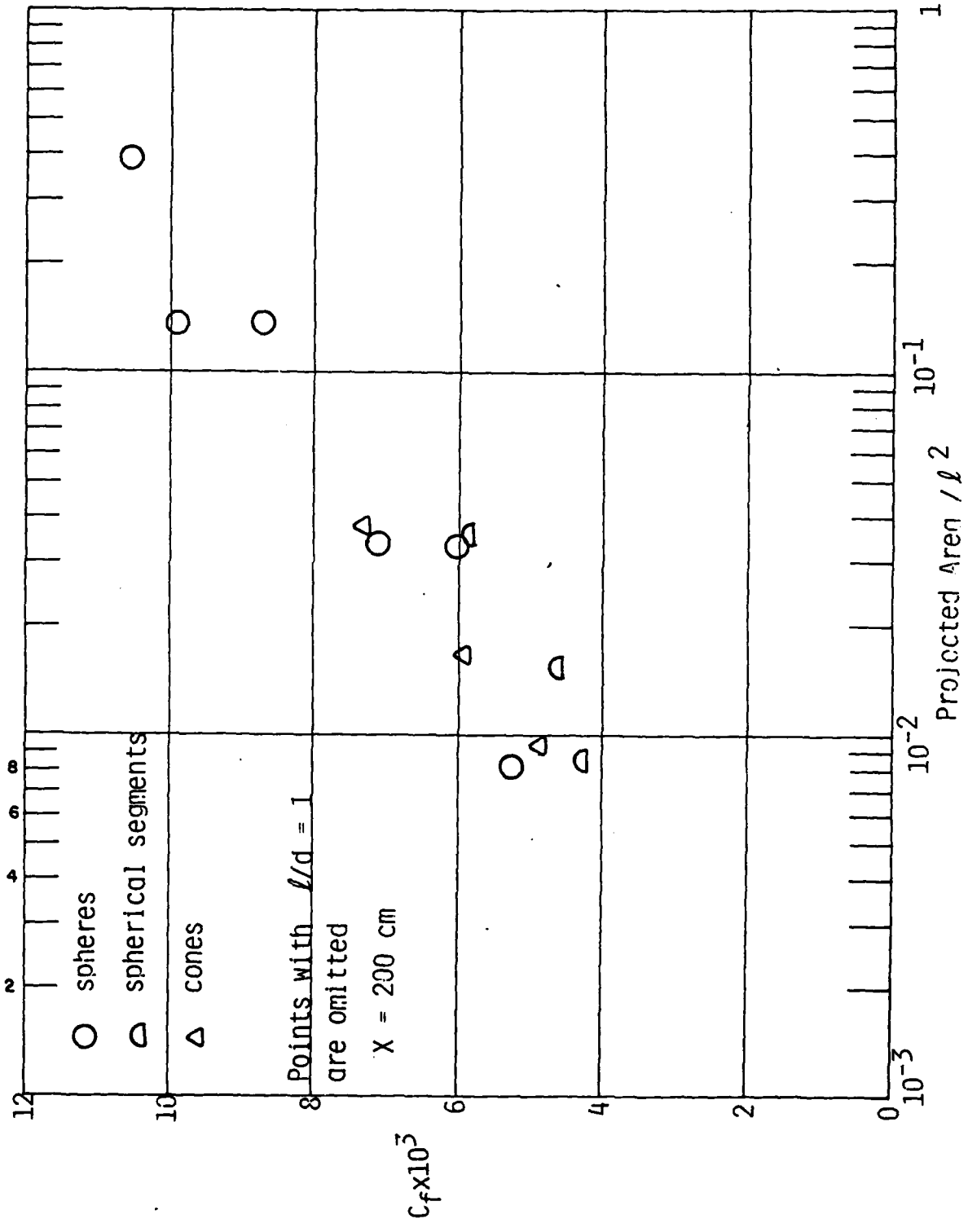


Fig. 14 Skin Friction vs. projected roughness area per unit surface area, according to Schlichting's data.

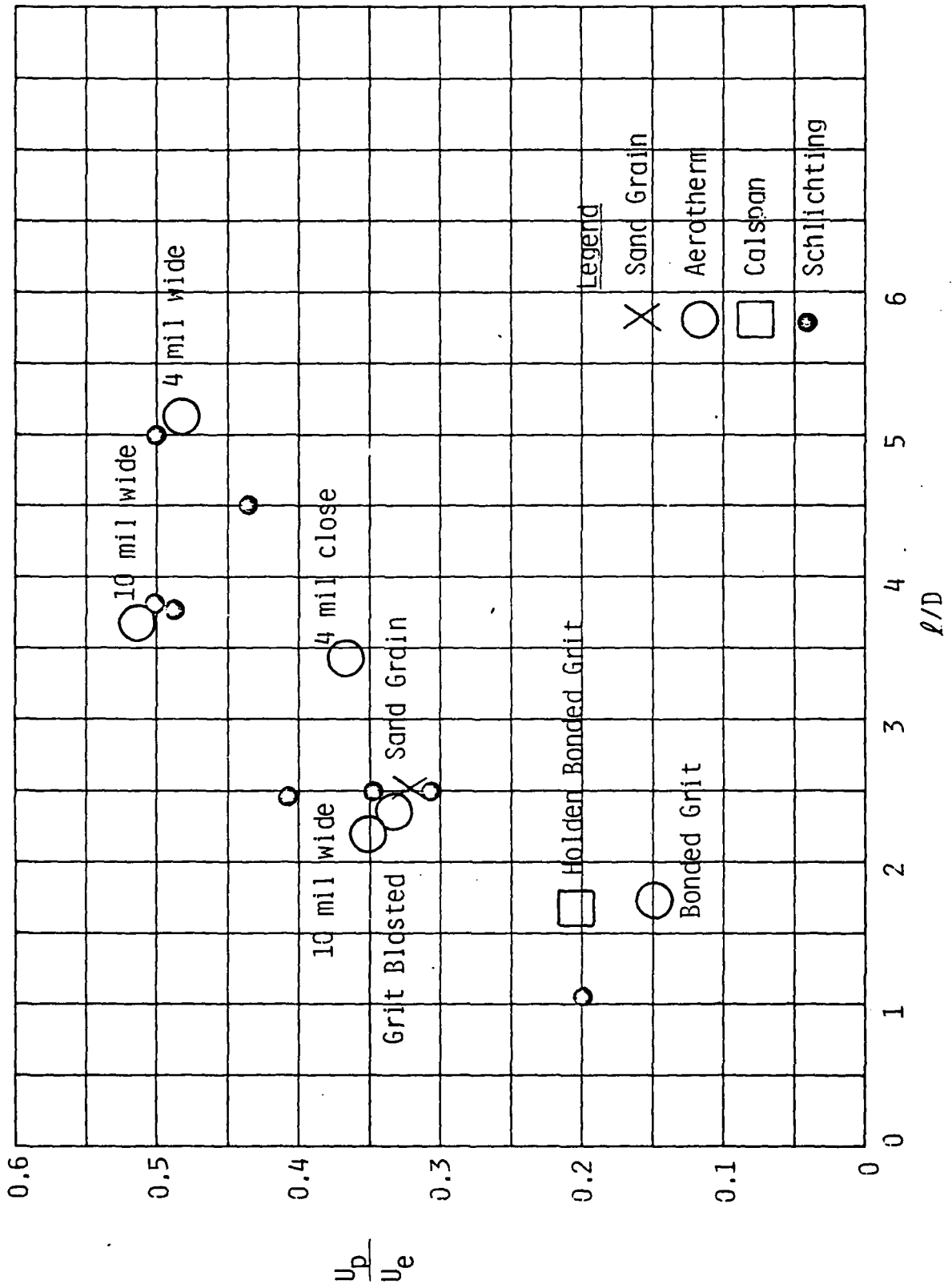


Fig. 15 Preliminary correlation of roughness "plateau" velocity versus roughness spacing at $Re=10^4$.

substantially. The only important terms are those representing dissipation and turbulent diffusion. Convection is always small for small y , the production terms are thoroughly negligible since $\partial U/\partial y \approx 0$, and laminar diffusion is considerably less than turbulent diffusion, at least for reasonably large roughness heights. The turbulence simply diffuses inward from the tops of the elements and is dissipated. This behavior may be contrasted with that in the wall region of a smooth wall boundary layer or above the elements of rough walls. There the production and dissipation terms are in balance, with convection and diffusion negligible. The nature of the computed rough wall boundary layer behavior suggests that a multi-layer method would be appropriate. Such a method would be similar to the two-layer treatment developed by Reeves¹⁵ for smooth wall turbulent boundary layers. In the rough wall case, there would be three regions: 1) the roughness region ($y < k$); 2) the law-of-the-wall region; and 3) the outer wake region. Such an approach would probably be sufficiently tractable from a computational viewpoint to be capable of use for engineering applications, but should be free of the empiricism usually associated with the simpler methods. The three regions are coupled, and the solution might involve a moderate effort. The development of such an approximate technique is well beyond the scope of this study, but is planned to be addressed in future efforts.

V. COMPARISONS WITH EXPERIMENTS AT HIGH MACH NUMBERS

Although the main emphasis of this study is on the effect of roughness character, the behavior of rough wall turbulent boundary layers at high edge Mach numbers, as well as with wall blowing, has also been examined. One possible issue is whether supersonic flow about the roughness elements can occur and alter the flowfield. The edge Mach number for the AEDC tests, discussed above, is only 1.7, so the velocity at the top of the elements is well subsonic and no significant effect of compressibility would have been expected. The combined influence of mass transfer and roughness is also unknown. A limited amount of data is available that can be analyzed with the present model to indicate the extent to which uncertainties exist.

The first high Mach number tests with distributed surface roughness were conducted by Keel⁸ on 5° sharp cones in Tunnel No. 2 at the Naval Surface Weapons Center. Sand grains were uniformly applied to the model with epoxy, yielding roughness heights of either 23 mils or 43 mils. Element spacing measurements were not reported, and we assumed a value ($\lambda/D = 2.5$) which is typical of the bonded grit surfaces constructed by Acurex⁷ and Calspan.⁹ The tests of primary interest were conducted at $M_\infty = 5$ or $M_e = 4.77$; skin friction and heat transfer were measured with floating element balances and slug calorimeter gauges, respectively.

One noteworthy aspect of Keel's experiment is that the measurements were obtained at a fixed station on the cone, $x = 2$ ft. The Reynolds number was varied by decreasing the tunnel pressure, and the results plotted as C_f or St vs Re_θ (see Figs. 16 and 17). The manner by which the data were collected must be recognized to properly interpret these results. With a smooth wall, C_f is a function only of Re_θ (assuming fixed values of M_e and T_w/T_e) and one may equally well traverse the C_f vs Re_θ curve by varying pressure (i.e., density) or distance (i.e., θ). However a second independent parameter enters with rough walls. For simplicity, let us follow Nikuradse,¹ Acurex,¹⁰ and our own work⁵ and use

$$k^+ = \rho_w u_\tau k / \mu_w$$

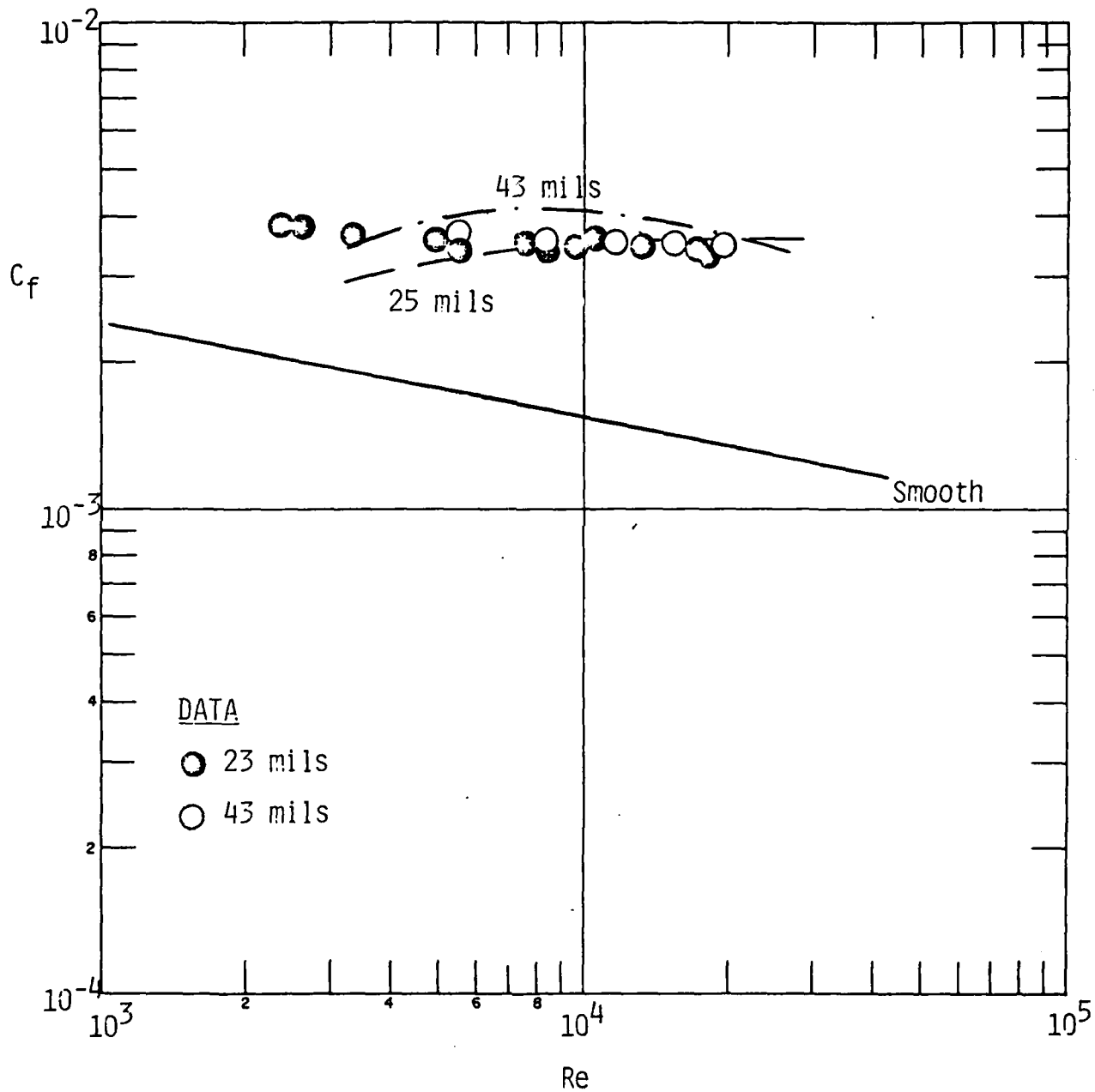


Fig. 16 Comparison with present theory with Keel's measurements at $M_e = 4.8$ with $k = 23$ and 43 mils.

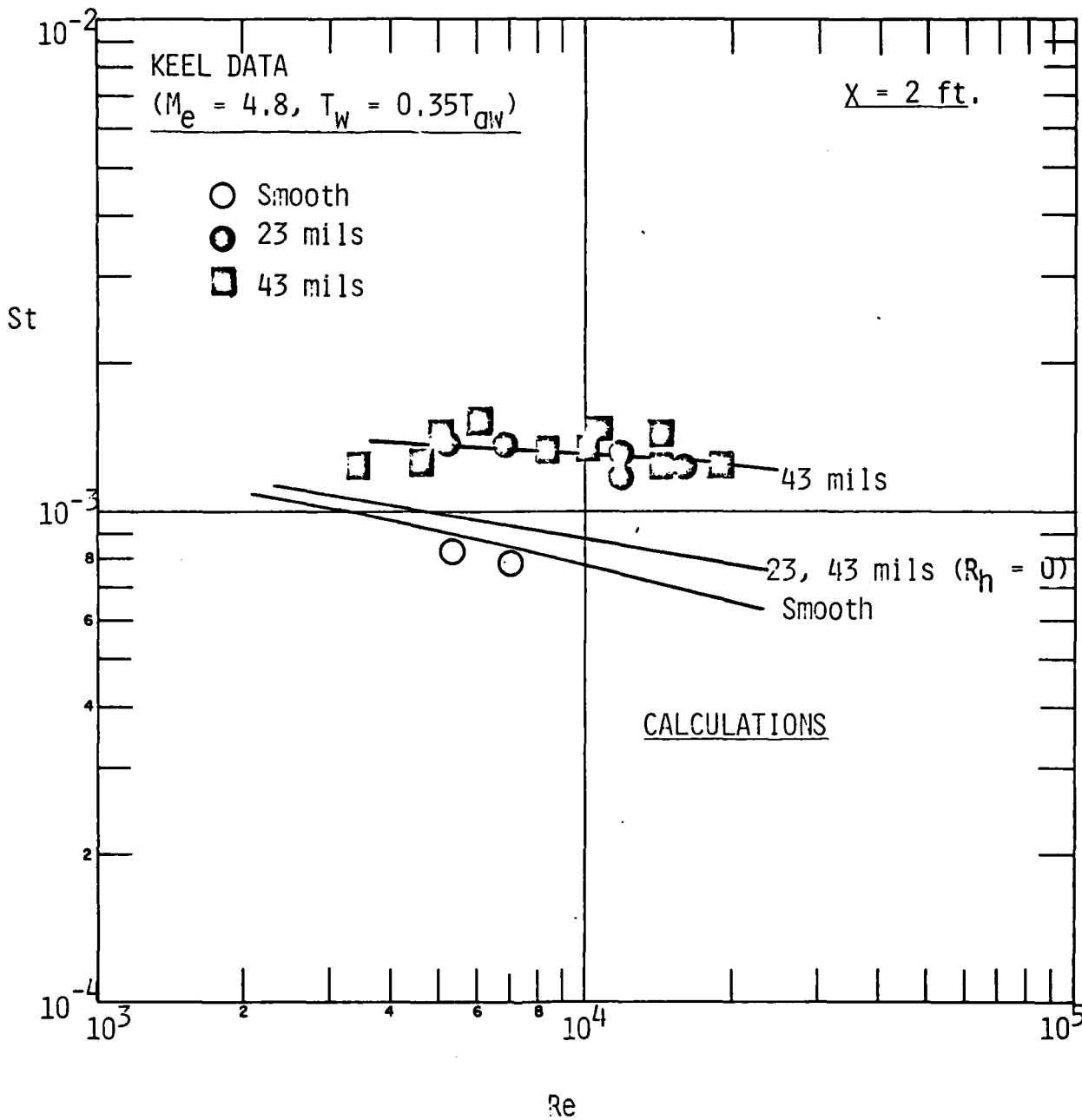


Fig. 17 Comparison of present theory with Keel's heat transfer data -
 $M_e = 4.8, k = 23 \text{ and } 43 \text{ mils.}$

as the fundamental parameter to describe the roughness augmentation effect. Furthermore, u_t/u_e is a very weak function of Re_θ and may be considered constant for the purposes of this argument. Thus, if we consider increasing distance along a flat plate or cone, Re_θ increases because $\theta \sim x^{0.8}$, while k^+ remains constant. Conversely, when Keel raises the pressure at a fixed station, both Re_θ and k^+ increase together, linearly with the density. This offers an explanation for the almost complete absence of slope for the data in Figs. 16 and 17; the increasing roughness augmentation (with increasing k^+) tends to cancel the natural tendency of C_f or St to decrease with increasing Re_θ .

Keel's procedure also complicates our computational tasks in comparing with his data. An individual computer run yields only one point (at the appropriate x station) that may properly be plotted against Keel's results. Thus, a number of runs were required to define the calculated curves of Figs. 16 and 17, whereas the calculations shown above in Figs. 6 through 13 required only one run per case. Agreement with the skin friction data is very good - k^+ is apparently sufficiently large that the roughness augmentation is nearly saturated and there is little difference between 23 and 43 mils. The heat transfer comparison is quite similar; note the importance of the source term in Eq. (2) which is required to conserve total enthalpy in the flow about an element.

Figure 18 shows the computed Mach number profile for the 23 mil case of Keel. The point of interest is that the Mach number is barely supersonic for $y \leq k$. Thus, shock waves about the elements might be expected. The presence of shock waves would not invalidate the drag term used in the model to describe the influence of roughness, since the drag coefficient would not be expected to depend strongly on Mach number. However, shock waves would cause the drag to be deposited on a range of streamlines. This smearing effect might be appreciable, although our current feeling is that local Mach numbers for $y < k$ will not become sufficiently supersonic for a large effect to occur. The agreement seen in Figs. 16 and 17 offers some support for this position. However, re-entry applications can easily involve edge Mach numbers of 8-10, and the current

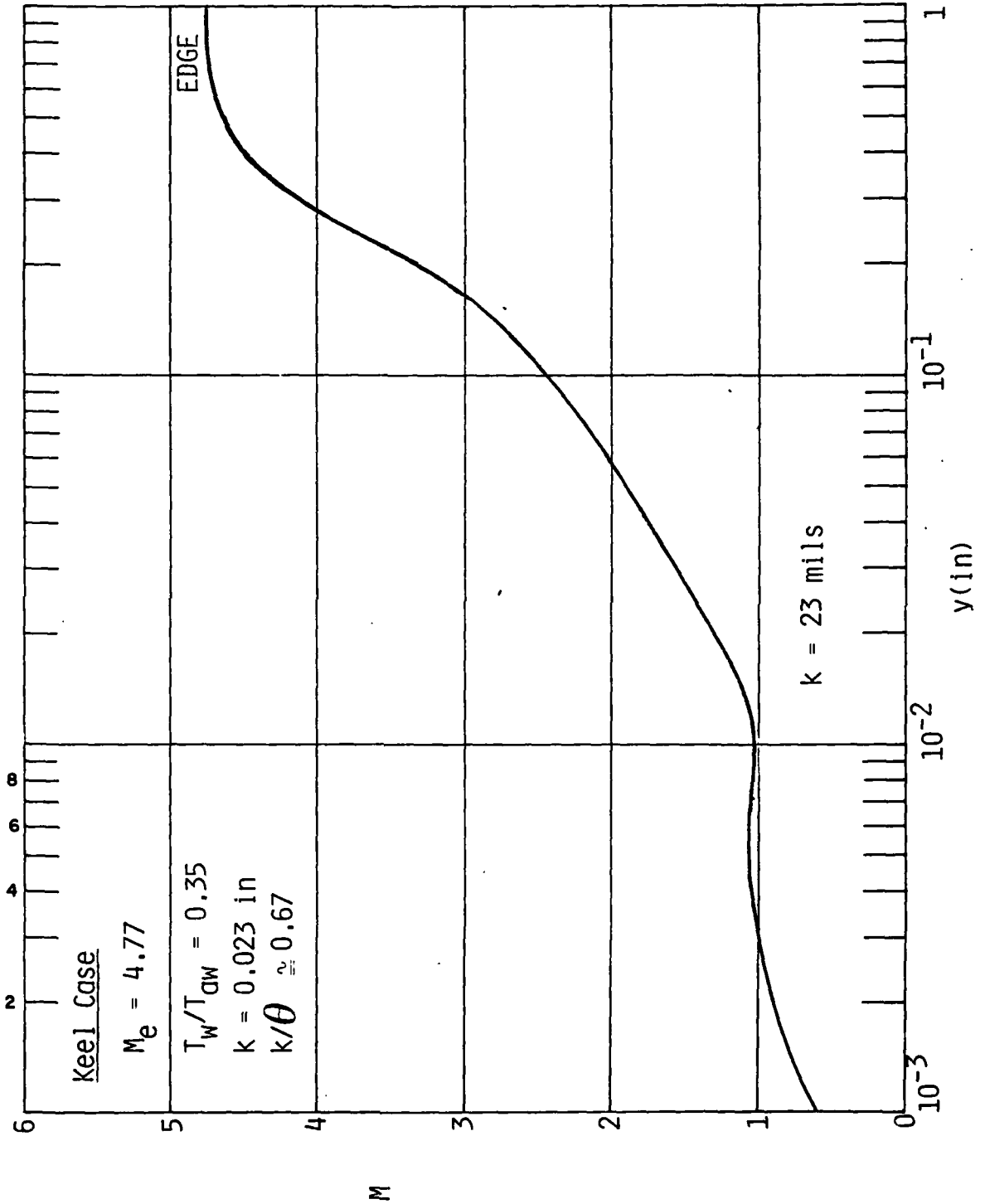


Fig. 18 - Computed boundary layer Mach number profile for $M_e = 4.8$, $k = 23 \text{ mils}$.

model will have to be verified in that range. It will be quite interesting to examine data at $M_e = 8-10$ as they become available, such as from the current efforts of Holden¹¹ at Calspan and Hill¹² at NSWC.

Finally, the limited data on the combined effect of roughness and blowing obtained by Voisinet¹³ have been examined. This experiment was performed on a wind tunnel wall under adiabatic conditions at $M = 3$ at NSWC. The value of the results is compromised by two factors: 1) screens were used to provide the surface roughness; and, 2) the measurements were also obtained at a fixed station by varying the pressure. The use of screens is unfortunate, but necessitated by the extreme difficulty in fabricating a roughened, porous model. The essentially two-dimensional nature of the screen wires may provide a poor simulation of distributed roughness, and the equivalent sand grain roughness is not known. We arbitrarily used the screen wire diameter as the equivalent roughness height; a somewhat larger value would have improved the limited comparisons, shown in Fig. 19. Note that the solid lines are Voisinet's data,¹³ while the squares give the computed skin friction at the appropriate station. The manner by which the data were obtained significantly complicates the data analysis, in that it is difficult to find a condition where roughness and blowing are simultaneously important. However, given the uncertainty in the appropriate value of k , the model predicts essentially the correct value for blow-off at $Re_\theta \approx 10^4$.

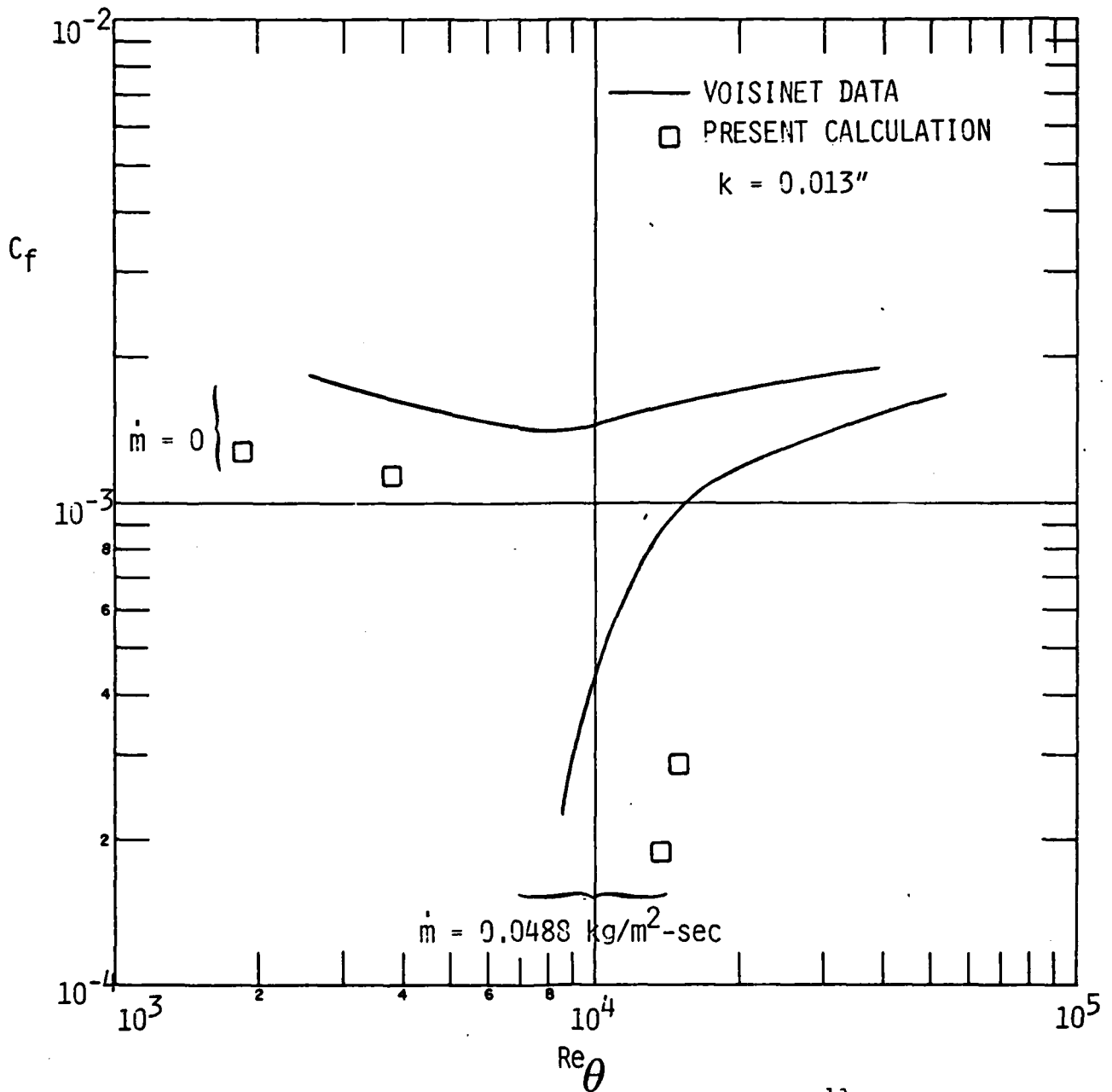


Fig. 19 - Comparison of present theory with Voisinet¹³ data on combined effect of roughness and mass addition.

VI. SUMMARY

The present theoretical approach to rough wall turbulent boundary layers has been compared with the available experimental data on the influence of roughness character (element shape and spacing). The theory treats roughness as distributed sources and sinks, primarily as a sink term for form drag in the mean momentum equation, and allows the element shape and spacing to be specified as input quantities. The blockage effect of closely spaced elements is treated by modifying the distributed roughness terms to account for the volume fraction occupied by the solid material.

Calculations based on the theory have been compared with the available sources of data where the roughness shape and spacing were varied. Reasonable agreement was obtained with most of the classic measurements of Schlichting on the side wall of a water tunnel, with spherical, spherical segment, and conical roughness elements of various relative spacings. The cone measurements imply a somewhat higher effective drag coefficient than observed on the other shapes. The second set of experiments that were analyzed in detail were performed by Acurex in AEDC Tunnel F under supersonic conditions. A number of surface roughnesses were created by grit or chemical etching processes. The heat transfer data, as well as the PSI theory, indicate spacing to be more important than height, at least under the conditions tested. The limited skin friction data obtained in these tests could not be interpreted unambiguously.

Analysis of the computer results reveals that the computed mean velocity profile is nearly constant over much of the height range $y < k$. This in turn indicates that the projected (frontal) roughness element area per unit superficial surface area is a key scaling parameter. The other important quantity, the value of the "plateau" velocity that applies for $y < k$, has been found to depend primarily on relative roughness spacing, at least according to a correlation of our computer output. The nature of the important processes in the range below the tops of the elements suggests a "three-layer" model, which could provide quite accurate predictions for roughness effects at a reasonable effort.

Finally, the quite limited available experimental measurements for hypersonic rough wall turbulent boundary layers, as well as for the combined effects of wall blowing and roughness, have been examined with the present theory. It will be interesting to determine if other processes, such as the influence of locally supersonic flow around the roughness elements, are important as more definitive data become available in the future.

REFERENCES

1. Nikuradse, J., "Strömungsgesetze in rauhen Rohren", VDI Forschungsheft, No. 361, SerB, Vol. 4, (1933); English Translation, NACA TM1292, 1950.
2. Schlichting, H., "Experimental Investigation of the Problem of Surface Roughness," NACA TM823 (1937). Also Boundary Layer Theory, McGraw-Hill, New York (1968).
3. Bettermann, D., "Contribution a l'Etude de la Connection Forcee Turbulente le Long de Plaques Rugueuses," Int. J. Heat & Mass Transfer 9, 153-164 (1966).
4. Dvorak, F.A., "Calculation of Turbulent Boundary Layers on Rough Surfaces in Pressure Gradient", AIAA Journal, Vol. 7, No. 9, Sept. 1969, pp. 1752-1759. Also AIAA J., Vol. 4, No. 11, Nov. 1972, pp. 1447-1451.
5. Finson, M.L. and Wu, P.K.S., "Analysis of Rough Wall Turbulent Heating with Application to Blunted Flight Vehicles," AIAA Paper 79-008 (1979). Also PSI TR-158, AFOSR-TR-79-0199.
6. Saffman, P.G. and Wilcox, D.C., "Turbulence-Model Predictions for Turbulent Boundary Layers," AIAA Journal, Vol. 12, No. 4, April 1974, pp. 541-546.
7. Foster, T., Read, D., and Murray, A., "Reduced Data Report: Surface Roughness Heating Augmentation Tests in AEDC Tunnel F., Vol. II," Accurex Report TR-79-183 (1979).
8. Keel, A.G., Jr., "Influence of Surface Roughness on Skin Friction and Heat Transfer for Compressible Turbulent Boundary Layers," AIAA Paper 77-178, (1977).
9. Holden, M.S., "Studies of the Effects of Transitional and Turbulent Boundary Layers on the Aerodynamic Performance of Hypersonic Re-entry Vehicles in High Reynolds Number Flows," Calspan Rep. AB-5834-A-2, AFOSR-TR-79-0125, (1978).
10. Dahm, T.J. et al., "Passive Noretip Technology (PANT II) Program, "SAMSO-TR-77-11, Oct. 1976, Acurex Corp., Mountain View, Calif.
11. Holden, M.S., Presentation at Roughness Effects Review Meeting, AF Flight Dynamics Lab, WPAFB, Dayton, Ohio, 10-11 October, 1979.

12. Hill, J.A.F., "Effects of Surface Roughness on R/V Frustum Heat Transfer, Quick-Work Report," Naval Surface Weapons Center, July 1979.
13. Voisinet, R.L.P., "Combined Influence of Roughness and Mass Transfer on Turbulent Skin Friction at Mach 2.9," AIAA paper 79-0003 (1979).
14. Van Driest, E.R., "Problem of Aerodynamic Heating," Aeronautical Engineering Review, 15, 26-41 (1956).
15. Reeves, B.L., "Two-Layer Model of Turbulent Boundary Layers," AIAA J. 12, 932-939 (1974).

APPENDIX

REYNOLDS STRESS MODEL EQUATIONS

The governing partial differential equations for the various turbulent quantities are listed here. For more details, the reader is referred to our previous report.⁵ In practice, it is convenient to replace u'^2, v'^2, w'^2 by the kinetic energy $q^2 = (u'^2 + v'^2 + w'^2)/2$ and two measures of the degree of anisotropy $S_{11} = u'^2 - 2/3 q^2, S_{22} = v'^2 - 2/3 q^2$.

For steady flow, the governing equations include continuity:

$$\frac{\partial}{\partial x_i} (\rho U_i) = 0 \quad (A-1)$$

the mean momentum equation:

$$\rho U_k \frac{\partial U}{\partial x_k} = - \frac{\partial \bar{p}}{\partial x} - \frac{\partial}{\partial y} (\rho \bar{uv}) + \frac{\partial}{\partial y} \left(\mu \frac{\partial U}{\partial y} \right) + R_u \quad (A-2)$$

and, for the five second-order quantities:

$$\begin{aligned} \rho U_k \frac{\partial q^2}{\partial x_k} = & - \rho \bar{uv} \frac{\partial U}{\partial y} - \rho \bar{q} + 0.2 \frac{\partial}{\partial y} \left[\rho \frac{q^2 v^2}{\bar{q}} \frac{\partial}{\partial y} (q^2 + v^2) \right] \\ & + \frac{\partial}{\partial y} \mu \frac{\partial q^2}{\partial y} + (S_{22} - S_{11}) \rho \frac{\partial U}{\partial x} + R_q \end{aligned} \quad (A-3)$$

$$\begin{aligned} \rho U_k \frac{\partial S_{11}}{\partial x_k} = & - \frac{14}{33} \rho \bar{uv} \frac{\partial U}{\partial y} - C_E \rho \frac{\bar{q}}{q} S_{11} + 0.2 \frac{\partial}{\partial y} \left[\rho \frac{q^2 v^2}{\bar{q}} \frac{\partial}{\partial y} (S_{11} - \frac{2}{3} v^2) \right] \\ & + \frac{\partial}{\partial y} \mu \frac{\partial S_{11}}{\partial y} - \rho \left[\frac{8}{15} q^2 + \frac{2}{33} S_{11} + \frac{1}{33} S_{22}' \right] \frac{\partial U}{\partial x} \end{aligned} \quad (A-4)$$

$$\rho U_k \frac{\partial S_{22}}{\partial x_k} = \frac{13}{33} \rho \overline{uv} \frac{\partial U}{\partial y} - C_E \rho \frac{\bar{\xi}}{2} S_{22} + 0.2 \frac{\partial}{\partial y} \left[\rho \frac{q^2 v^2}{\bar{\xi}} \frac{\partial}{\partial y} (S_{22} - \frac{4}{3} v^2) \right]$$

$$+ \frac{\partial}{\partial y} \mu \frac{\partial S_{22}}{\partial y} + \rho \left[\frac{8}{15} q^2 + \frac{1}{33} S_{11} + \frac{2}{33} S_{22} \right] \frac{\partial U}{\partial x} \quad (A-5)$$

$$\rho U_k \frac{\partial \overline{uv}}{\partial x_k} = - \rho \left[\frac{4}{15} q^2 - \frac{2}{11} S_{11} + \frac{5}{22} S_{22} \right] \frac{\partial U}{\partial y} - C_E \rho \frac{\bar{\xi}}{2} \overline{uv}$$

$$+ 0.4 \frac{\partial}{\partial y} \left[\rho \frac{q^2 v^2}{\bar{\xi}} \frac{\partial \overline{uv}}{\partial y} \right] + \frac{\partial}{\partial y} \mu \frac{\partial \overline{uv}}{\partial y} \quad (A-6)$$

$$\rho U_k \frac{\partial \bar{\xi}}{\partial x_k} = - 1.25 \rho \frac{\overline{uv}}{2} \frac{\partial U}{\partial y} \bar{\xi} - C_{\bar{\xi}} \rho \frac{\bar{\xi}^2}{2} + 177.6 \rho \frac{v^2 q^2}{y^4}$$

$$+ 0.322 \frac{\partial}{\partial y} \left[\rho \frac{q^2 v^2}{\bar{\xi}} \frac{\partial \bar{\xi}}{\partial y} \right] + \frac{\partial}{\partial y} \mu \frac{\partial \bar{\xi}}{\partial y} - 1.25 \rho \frac{u^2}{2} \frac{\partial U}{\partial x} \bar{\xi} + R_{\bar{\xi}} \quad (A-7)$$

$$\text{where } C_E = \frac{1.2 + 12.5 \pi / \text{Re}_\Lambda}{1 + 12.5 \pi / \text{Re}_\Lambda},$$

$$C_{\bar{\xi}} = \frac{\left(0.288 + 6.6 \pi / \text{Re}_\Lambda + 35 \pi^2 / \text{Re}_\Lambda^2 \right)}{\left(0.4 + 5 \pi / \text{Re}_\Lambda \right)^2}$$

and Re_Λ is the turbulent Reynolds number $q\Lambda/\nu$, with Λ being related to the dissipation rate by

$$\xi = 0.4 \frac{q}{\Lambda} + 5 \pi v \frac{q}{2} = 0.4 \frac{q}{\Lambda} (1 + 12.5 \pi / \text{Re}_\Lambda) \quad (\text{A-8})$$

the corresponding equations for enthalpy-related quantities are:

$$\rho \frac{D\bar{h}}{Dt} = \bar{U}_i \frac{\partial \bar{p}}{\partial x_i} - \frac{\partial}{\partial y} (\rho \bar{v}'h') + \frac{1}{\text{Pr}} \frac{\partial}{\partial y} \left(\mu \frac{\partial \bar{h}}{\partial y} \right) + \mu \left(\frac{\partial U}{\partial y} \right)^2 + \rho \xi \quad (\text{A-9})$$

$$\begin{aligned} \rho \frac{D\overline{h'^2}}{Dt} &= -2 \rho \bar{v}'h' \frac{\partial \bar{h}}{\partial y} - C_{T_1} \rho \frac{\xi}{q} \overline{h'^2} + 0.40 \frac{\partial}{\partial y} \left(\rho \frac{q^2 v^2}{\xi} \frac{\partial \overline{h'^2}}{\partial y} \right) \\ &+ \frac{1}{\text{Pr}} \frac{\partial}{\partial y} \left(\mu \frac{\partial \overline{h'^2}}{\partial y} \right) \end{aligned} \quad (\text{A-10})$$

$$\begin{aligned} \rho \frac{D\overline{v'h'}}{Dt} &= -\rho v^2 \frac{\partial \bar{h}}{\partial y} - 0.09835 \bar{\rho} \overline{u'h'} \frac{\partial U}{\partial y} - C_{T_2} \rho \frac{\xi}{q} \overline{v'h'} \\ &+ 0.80 \frac{\partial}{\partial y} \left(\rho \frac{q^2 v^2}{\xi} \frac{\partial \overline{v'h'}}{\partial y} \right) + \frac{1}{\text{Pr}} \frac{\partial}{\partial y} \left(\mu \frac{\partial \overline{v'h'}}{\partial y} \right) \end{aligned} \quad (\text{A-11})$$

$$\begin{aligned} \rho \frac{D\overline{u'h'}}{Dt} &= -0.3989 \bar{\rho} \overline{v'h'} \frac{\partial U}{\partial y} - \rho \bar{u}v \frac{\partial \bar{h}}{\partial y} - C_{T_2} \rho \frac{\xi}{q} \overline{u'h'} \\ &+ 0.40 \frac{\partial}{\partial y} \left(\rho \frac{q^2 v^2}{\xi} \frac{\partial \overline{u'h'}}{\partial y} \right) + \frac{1}{\text{Pr}} \frac{\partial}{\partial y} \left(\mu \frac{\partial \overline{u'h'}}{\partial y} \right) \end{aligned} \quad (\text{A-12})$$

$$\text{where } C_{T_1} = \frac{0.8 + 7.5 \pi / \text{Re}_\Lambda}{1 + 12.5 \pi / \text{Re}_\Lambda}$$

$$C_{T_2} = \frac{1.165 + 12.5 \pi / \text{Re}_\Lambda}{1 + 12.5 \pi / \text{Re}_\Lambda}$$

The terms R_u , R_h , R_q , and R_ϕ contain the effect of roughness on the boundary layer. For the mean velocity and enthalpy equations, R_u and R_h were presented in Eqs. (1) and (2) in Section II, the other two terms are source terms for kinetic energy and dissipation, describing the fluctuations introduced in the wakes of elements. For the fully turbulent boundary layers considered in this study, these terms are generally small compared to the natural turbulence production terms. As described in Ref. 5, the terms used are:

$$R_q = 0.04 \rho U^3 D / \ell^2 \quad (\text{A-13})$$

$$R_\phi = 0.04 \rho U^3 \nu / D \ell^2 \quad (\text{A-14})$$

UNCLASSIFIED

SECURITY CLASSIFICATION OF THIS PAGE (When Data Entered)

REPORT DOCUMENTATION PAGE		READ INSTRUCTIONS BEFORE COMPLETING FORM
1. REPORT NUMBER AFOSR-TR- 80 - 0251	2. GOVT ACCESSION NO.	3. RECIPIENT'S CATALOG NUMBER
4. TITLE (and Subtitle) ROUGH WALL REENTRY HEATING ANALYSIS Effect of Surface Roughness Character on Turbulent Boundary Layer Heating		5. TYPE OF REPORT & PERIOD COVERED FINAL 1 Dec 1977 - 30 Sep 1979
7. AUTHOR(s) M L FINSON A S CLARKE P K S WU		6. PERFORMING ORG. REPORT NUMBER PSI TR-204
9. PERFORMING ORGANIZATION NAME AND ADDRESS PHYSICAL SCIENCES, INC 30 COMMERCE WAY WOBURN, MA 01801		8. CONTRACT OR GRANT NUMBER(s) F49620-78-C-0028
11. CONTROLLING OFFICE NAME AND ADDRESS AIR FORCE OFFICE OF SCIENTIFIC RESEARCH/NA BLDG 410 BOLLING AFB DC 20332		10. PROGRAM ELEMENT, PROJECT, TASK AREA & WORK UNIT NUMBERS 2307A1 61102F
14. MONITORING AGENCY NAME & ADDRESS (if different from Controlling Office)		12. REPORT DATE February 1980
		13. NUMBER OF PAGES 45
		15. SECURITY CLASS. (of this report) UNCLASSIFIED
		15a. DECLASSIFICATION/DOWNGRADING SCHEDULE
16. DISTRIBUTION STATEMENT (of this Report) Approved for public release; distribution unlimited.		
17. DISTRIBUTION STATEMENT (of the abstract entered in Block 20, if different from Report)		
18. SUPPLEMENTARY NOTES		
19. KEY WORDS (Continue on reverse side if necessary and identify by block number) TURBULENT BOUNDARY LAYER TURBULENT HEAT TRANSFER REENTRY HEATING		
20. ABSTRACT (Continue on reverse side if necessary and identify by block number) A Reynolds stress model is used to evaluate the effect of surface roughness on turbulent boundary layers. Roughness is represented by distributed source or sink terms in the various governing equations, the most important term being a sink term in the mean momentum equation describing firm drag on the roughness elements. The blockage effect of closely spaced elements is treated by accounting for the volume fraction occupied by the solid material. Calculations based on the theory have been compared with the available data on the influence of roughness character, where the roughness shape and spacing were varied.		

DD FORM 1473
1 JAN 73

UNCLASSIFIED

UNCLASSIFIED

SECURITY CLASSIFICATION OF THIS PAGE (When Data Entered)

Reasonable agreement was obtained against most of Schlichting's low speed data with spherical, spherical segment, and conical roughness elements at various spacings. The cone measurements imply a somewhat higher effective drag coefficient than observed on the other shapes. The second set of experiments that were analyzed in detail were performed by Acurex under supersonic conditions, with a number of roughnesses created by grit or chemical etching processes. The heat transfer data and the present theory indicate spacing to be more important than height under the conditions tested. Analysis of the computer results reveals that the mean velocity is nearly constant over much of the height range $y < k$. This in turn indicates that the projected roughness element area per unit superficial area is a key scaling parameter. The "plateau" velocity is found to depend primarily on relative roughness spacing, and methods are suggested for developing better approximate techniques for predicting roughness character effects. Finally, preliminary data on hypersonic rough wall turbulent boundary layers have been examined with the present theory.

UNCLASSIFIED